The use of QBO, ENSO and NAO perturbations in the evaluation of GOME-2/MetopA total ozone measurements

Kostas Eleftheratos[1,2], Christos S. Zerefos[2,3,4,5], Dimitris S. Balis[6], Maria-Elissavet Koukouli[6], John Kapsomenakis[3], Diego G. Loyola[7], Pieter Valks[7], Melanie Coldewey-Egbers[7], Christophe Lerot[8], Stacey M. Frith[9], Amund S. Haslerud[10], Ivar S. A. Isaksen[10,11], Seppo Hassinen[12]

[1]Laboratory of Climatology and Atmospheric Environment, Faculty of Geology and Geoenvironment, National and Kapodistrian University of Athens, Greece
[2]Biomedical Research Foundation of the Academy of Athens, Athens, Greece
[3]Research Centre for Atmospheric Physics and Climatology, Academy of Athens, Athens, Greece
[4]Mariolopoulos-Kanaginis Foundation for the Environmental Sciences, Athens, Greece
[5]Navarino Environmental Observatory (N.E.O.), Messinia, Greece
[6]Laboratory of Atmospheric Physics, Department of Physics, Aristotle University of Thessaloniki, Greece
[7]Institut für Methodik der Fernerkundung (IMF), Deutsches Zentrum für Luft- und Raumfahrt (DLR), Oberpfaffenhofen, Germany
[8]Royal Belgian Institute for Space Aeronomy (BIRA), Brussels, Belgium
[9]Science Systems and Applications, Inc., Lanham, MD, USA
[10]Cicero Center for International Climate Research, Oslo, Norway
[11]Department of Geosciences, University of Oslo, Oslo, Norway
[12]Finnish Meteorological Institute, Helsinki, Finland

Correspondence to: Kostas Eleftheratos (kelef@geol.uoa.gr)

Abstract. In this work we present evidence that quasi cyclical perturbations in total ozone (Quasi Biennial Oscillation (QBO), El Nino Southern Oscillation (ENSO) and North Atlantic Oscillation (NAO)) can be used as independent proxies in evaluating Global Ozone Monitoring Experiment-2 aboard MetopA (GOME-2A) satellite total ozone data, using ground-based measurements, other satellite data and chemical transport model calculations. The analysis is performed in the frame of the validation strategy on longer time scales within the European Organisation for the Exploitation of Meteorological Satellites (EUMETSAT), Satellite Application Facility on Atmospheric Composition Monitoring (AC SAF) project, and covers the period 2007-2016. Comparison of GOME-2A total ozone with ground observations shows mean differences of about –0.7 ± 1.4% in the tropics (0-30 deg.), about +0.1 ± 2.1% in mid-latitudes (30-60 deg.), and about +2.5 ± 3.2% and 0.0 ± 4.3% over the northern and southern high latitudes (60-80 deg.), respectively. In general, we find that GOME-2A total ozone data depict the QBO/ENSO/NAO natural fluctuations in concurrence with co-located Solar Backscatter Ultraviolet Radiometer (SBUV), GOME-type Total Ozone Essential Climate Variable (GTO-ECV; composed of total ozone observations from GOME (Global Ozone Monitoring Experiment), SCIAMACHY (SCanning Imaging Absorption SpectroMeter for Atmospheric CHartographY), GOME-2A, and OMI (Ozone Monitoring Instrument) combined into one homogeneous time series) and ground-based (GB) observations. Total ozone from GOME-2A is well correlated with the QBO (highest correlation in the tropics of +0.8) in agreement with SBUV, GTO-ECV and GB data which also give the highest correlation in the tropics. The differences between deseazonalised GOME-2A and GB total ozone in the tropics are within ±1%. These differences were tested further as to their correlations with the QBO. The differences had practically no QBO signal, providing an independent test of the stability of the long-term variability

of the satellite data. Correlations between GOME-2A total ozone and the Southern Oscillation Index (SOI) were studied over the tropical Pacific Ocean after removing seasonal, QBO and solar cycle related variability. Correlations between ozone and SOI are on the order of +0.5, consistent with SBUV and GB observations. Differences between GOME-2A and GB measurements at the station of Samoa (American Samoa; 14.25^{o} S, 170.6^{o} W) are within ±1.9%. We also studied the impact of NAO on total ozone in the northern mid-latitudes in winter. We find very good agreement between GOME-2A and GB observations over Canada and Europe as to their NAO-related variability, with mean differences reaching the ±1% levels. The agreement and small differences which were found between the independently produced total ozone data sets as to the influence of QBO, ENSO and NAO show the importance of these climatological proxies as additional tool for monitoring the long-term stability of satellite-ground truth biases.

1 Introduction

Ozone is an important gas of the Earth's atmosphere. In the stratosphere, ozone is considered *good ozone* because it absorbs ultraviolet-B radiation from the Sun, thus protecting the biosphere from a large part of the Sun's harmful radiation (e.g. Eleftheratos et al., 2012; Hegglin et al., 2015). In the lower atmosphere and near the surface, natural ozone has an equally important beneficial role because it initiates the chemical removal of air pollutants from the atmosphere such as carbon monoxide, nitrogen oxides and methane. Above natural levels however, ozone is considered *bad ozone* because it can harm humans, plants and animals. In addition, ozone is a greenhouse gas, warming the Earth's surface. In both the stratosphere and the troposphere, ozone absorbs infrared radiation emitted from Earth's surface, trapping heat in the atmosphere. As a result, increases or decreases in stratospheric or tropospheric ozone induce a climate forcing (Hegglin et al., 2015).

Ozone in the atmosphere can be measured by ground-based instruments, balloons, aircraft and satellites and can be calculated by chemical transport model (CTM) simulations. Measurements by satellites from space provide ozone profiles and column amounts over nearly the entire globe on a daily basis (e.g. WMO, 2014). The three Global Ozone Monitoring Experiment-2 (GOME-2) instruments carried on Metop platforms A, B and C serve this purpose. The first was launched on 19 October 2006, the second on 19 September 2012 and the last on 7 November 2018. The three GOME-2 instruments will provide unique long-term data sets of more than 15 years (2007-2024) related to atmospheric composition and surface ultraviolet radiation using consistent retrieval techniques (Hassinen et al., 2016). The GOME-2 off-line data is set to make a significant contribution towards climate and atmospheric research while providing near real-time data for use in weather forecasting and air quality forecasting applications (Hassinen et al., 2016).

Validation of satellite ozone measurements is performed with ground-based (GB) measurements as well as other satellite instruments (Hassinen et al., 2016). Validation of GOME-2A total ozone for the period 2007-2011 was performed by Loyola et al. (2011) and Koukouli et al. (2012). It was found that GOME-2 total ozone data agree at the ±1% level with GB measurements and other satellite data sets (Hassinen et al., 2016). The consistency between GOME-2A and GOME-2B total ozone columns, including a validation with GB measurements, was presented by

Hao et al. (2014). An updated time series of the differences between GOME-2A and GOME-2B with GB observations can be found in Hassinen et al. (2016). The long-term stability of the two satellite instruments was also noted in that study. Both satellites are consistent over the Northern Hemisphere with negligible latitudinal dependence, while over the Southern Hemisphere there is a systematic difference of 1% between the two satellite instruments (Hassinen et al., 2016).

Chiou et al. (2014) compared zonal mean total column ozone inferred from three independent multi-year data records, namely, SBUV (v8.6) total ozone (McPeters et al., 2013), GOME-type Total Ozone Essential Climate Variable (GTO-ECV) (Coldewey-Egbers et al., 2015; Garane et al., 2018), and GB total ozone for the period 1996-2011. Their analyses were conducted for the latitudinal zones of 0-30^{o} S, 0-30^{o} N, 50-30^{o} S, and 30-60^{o} N. It was found that, on average, the differences in monthly zonal mean total ozone vary between -0.3 and 0.8% and are well within 1%. In that study it was concluded that despite the differences in the satellite sensors and retrievals methods, the SBUV v8.6 and GTO-ECV data records show very good agreement both in the monthly zonal mean total ozone and the monthly zonal mean anomalies between 60°S and 60°N. The GB zonal means showed larger scatter in the monthly mean data compared to satellite-based records, but the scatter was significantly reduced when seasonal zonal averages were analysed. The differences between SBUV and GB total ozone data presented in Chiou et al. (2014) are well in agreement with Labow et al. (2013), who systematically compared SBUV (v8.6) total ozone data with that measured by Brewer and Dobson instruments at various stations as a function of time, satellite solar zenith angle, and latitude. The comparisons showed good agreement (within ±1%) over the past 40 years with very small bias approaching zero over the last decade. Comparisons with ozone sonde data showed good agreement in the integrated column up to 25 hPa with differences not exceeding 5% (Labow et al., 2013).

The observed small biases (at the percentage level) between satellite and GB observations of total ozone, as have been documented in the above studies, ensure the provision of accurate satellite ozone measurements. The high accuracy and stability of the satellite instruments is essential for monitoring the expected recovery of the ozone layer resulting from measures adopted by the 1987 Montreal protocol and its amendments (e.g., Zerefos et al., 2009; Loyola et al., 2011; Solomon et al., 2016; de Laat et al., 2017; Kuttippurath and Nair, 2017; Pazmiño et al., 2018; Stone et al., 2018; Strahan and Douglass, 2018). It is known that total ozone varies strongly with latitude and longitude as a result of chemical and transport processes in the atmosphere. Total ozone also varies with season. Seasonal variations are larger over middle and high latitudes and smaller in the tropics (e.g. WMO, 2014). On longer time scales total ozone variability is related to large scale natural oscillations such as the Quasi-Biennial Oscillation (QBO) (e.g. Zerefos et al., 1983; Baldwin et al., 2001), the El Nino Southern Oscillation (ENSO) (e.g. Zerefos et al., 1992; Oman et al., 2013; Coldewey-Egbers et al., 2014), the North Atlantic Oscillation (NAO) (e.g. Ossó et al., 2011; Chehade et al., 2014) and the 11-year solar cycle (e.g. Zerefos et al., 2001; Tourpali et al., 2007; Brönniman et al., 2013). Moreover, volcanic eruptions may also alter the thickness of the ozone layer (Zerefos et al., 1994; Frossard et al., 2013; Rieder et al., 2013; WMO, 2014). These natural perturbations affect the background atmosphere and consequently the distribution of the ozone layer. In this context, the study of the effect of known natural fluctuations in total ozone could serve as additional tool for evaluating the long-term variability of satellite total ozone data records.

The objective of the present work is to examine the ability of the GOME-2A total ozone data to capture the variability related to dynamical proxies of global and regional importance such as the QBO, ENSO and NAO, in comparison to GB measurements, other satellite data and model calculations. The variability of total ozone from GOME-2A is compared with the variability of total ozone from the other examined data sets during these naturally-occurring fluctuations in order to evaluate the ability of GOME-2A to depict natural perturbations. The analysis is performed in the frame of the validation strategy of GOME-2A data on longer time scales within the project of EUMETSAT, AC SAF. The evaluation of GOME-2A data performed here includes the study of monthly means of total ozone, the annual cycle of total ozone, the amplitude of the annual cycle [i.e., (max-min)/2], the relation with the QBO (correlation with zonal wind at the equator at 30 hPa), the relation with ENSO (correlation with SOI) and the relation with the NAO (correlation with the NAO index in winter (DJF mean)).

The annual cycle describes regular oscillations in total ozone that occur from month to month within a year. In general, month-to-month variations of total ozone are larger in middle and high latitudes than in the tropics. The QBO dominates the variability of the equatorial stratosphere (~16-50 km) and is easily seen as downward propagating easterly and westerly wind regimes, with a variable period averaging approximately 28 months. Circulation changes induced by the QBO affect temperature and chemistry (Baldwin et al., 2001). ENSO and NAO are naturally-occurring patterns or modes of atmospheric and oceanic variability, which orchestrate large variations in climate over large regions with profound impacts on ecosystems (Hurrell and Deser, 2009). We present the level of agreement between satellite-derived GOME-2A and GB total ozone in depicting natural oscillations like QBO, ENSO and NAO, highlighting the importance of these climatological proxies to be used as additional tools for monitoring the long-term stability of satellite-ground truth biases.

2 Data sources

The analysis uses GOME-2 satellite total ozone columns for the period 2007-2016. This data forms part of the operational EUMETSAT AC SAF GOME-2/MetopA GDP4.8 data product provided by the German Aerospace Center (DLR). The GOME-2 total ozone data have been monthly averaged on a 1^{o}x1^{o} latitude longitude grid. The overview of the GOME-2A satellite instrument and of the GOME-2 atmospheric data provided by AC SAF can be found in Hassinen et al. (2016).

To examine the natural variability of ozone on longer time scales, we have additionally analysed the GOME/ERS-2, SCIAMACHY/Envisat, GOME-2A, and OMI/Aura merged prototype level 3 harmonized data record (GTO-ECV, 1^{o}x1^{o}) for the period 1995-2016 (Coldewey-Egbers et al., 2015; Garane et al., 2018). This GTO-ECV ozone data product was generated and provided by DLR as part of the European Space Agency Ozone Climate Change Initiative (ESA O3 CCI) project. The ESA O3 CCI merged level-3 record, which is based on GOME/SCIAMACHY/GOME-2A/OMI level-2 data, was obtained using the GODFIT v3.0 retrieval algorithm. More on ESA O3 CCI datasets can be found in the studies by Van Roozendael et al. (2012), Lerot et al. (2014), Koukouli et al. (2015) and Garane et al. (2018).

Both datasets are compared with a combined TOMS/OMI/OMPS satellite total ozone data set constructed using data from the Total Ozone Mapping Spectrometer (TOMS) on Nimbus 7 (1979-1993), TOMS on Meteor 3 (1991-1994), TOMS on Earth Probe (1996-2005), the Ozone Monitoring Instrument (OMI) onboard the NASA Earth Observing System (EOS) Aura satellite (2005-present) and data from the next generation Ozone Mapping Profiler Suite (OMPS) nadir profiler instrument, launched in October 2011 on the Suomi National Polar-orbiting Partnership (NPP) satellite (McPeters et al., 2015). The total ozone data are available at 1^o x 1.25^o (TOMS) or 1^o x 1^o (OMI/OMPS) resolution from https://acd-ext.gsfc.nasa.gov/anonftp/toms/ (last access: 15 June 2018). From these data we constructed monthly mean total ozone data on a 5^o x 5^o grid. To account for known biases between the instruments (e.g., Labow et al., 2013) we use the Solar Backscatter Ultraviolet (SBUV) version 8.6 Merged Ozone Data Set (MOD) monthly zonal mean total ozone (https://acd-ext.gsfc.nasa.gov/Data_services/merged/index.html, also see next paragraph; last access: 15 June 2018) as a reference. We adjust each instrument such that the zonal mean in each 5^o band averaged over the instrument lifetime matches the corresponding SBUV MOD zonal mean average. Thus the inherent longitudinal variability is retained from the TOMS/OMI/OMPS measurements but any latitude-dependent bias between the instruments is removed. With the exception of Meteor 3 TOMS in the northern hemisphere, all offsets were within 2% at low and mid-latitudes. Such a data set should not be used for long-term trends but is sufficient for analyzing periodic variability such as QBO, ENSO and NAO. We used data for the period 1995-2016. We note here that another long-term data set which has been analysed for QBO, ENSO, NAO and other perturbations comes from the Multi-Sensor Reanalysis (Knibbe et el., 2014), but is not examined here.

In addition, we compare with satellite SBUV station overpass data from 1995 to 2016. The satellite data are based on measurements from three SBUV-type instruments from April 1970 to the present (continuous data coverage from November 1978). Even though the time series includes different versions of the SBUV instrument, the basic measurement technique remains the same over the advancement of the instrument from the Backscatter Ultraviolet (BUV) to SBUV/2 (Bhartia et al., 2013). Satellite overpass data over various ground-based stations are provided per day from https://acd-ext.gsfc.nasa.gov/anonftp/toms/sbuv/MERGED/ (last access: 15 June 2018). These overpass data are analogous to the SBUV MOD monthly zonal mean data previously mentioned. Both are constructed by first filtering lesser quality measurements and then averaging data from individual satellites when more than one instrument is operating. Monthly averages have been calculated by averaging the daily merged ozone overpass data for stations listed in Supplement Table S1. Details about the data are provided by McPeters et al. (2013) and Frith et al. (2014).

We also compare with GB observations of total ozone from a number of stations contributing to the World Ozone and Ultraviolet Radiation Data Centre (WOUDC). The WOUDC data centre is one of six World Data Centres which are part of the Global Atmosphere Watch programme of the World Meteorological Organization (WMO). The WOUDC data centre is operated by the Meteorological Service of Canada, a branch of Environment Canada. In total, we analysed total ozone daily summaries from 193 ground-based stations operating either Brewer, Dobson, filter, SAOZ or microtops instruments. The GB total ozone measurements are available from the website https://woudc.org/archive/Summaries/TotalOzone/Daily_Summary/ (last access: 15 June 2018). The various stations used in this study are listed in Table S1.

We have also analysed simulations of total ozone from the global 3-D chemical transport model (CTM) Oslo CTM3 (Søvde et al., 2012). The Oslo CTM3 has traditionally been driven by 3-hourly meteorological forecast data from the European Centre for Medium-Range Weather Forecasts (ECMWF) Integrated Forecast System (IFS) model, whereas in this study we apply the OpenIFS model (https://software.ecmwf.int/wiki/display/OIFS/) (last access: 15 June 2018), cycle 38r1, which is an improvement from Søvde et al. (2012). Details on the model are given in Søvde et al. (2012). The Oslo CTM3 comprises both detailed tropospheric and stratospheric chemistry. Photochemistry is calculated using fast-JX version 6.7c (Prather, 2012), and chemical kinetics from JPL 2010 (Sander et al., 2011). Total ozone columns compare well with measurements and other model studies (Søvde et al., 2012 and references therein). The horizontal resolution of the model is 2.25^{o} x 2.25^{o}. We used the global monthly mean total ozone columns for the period 1995-2016.

To examine the QBO component on total ozone we made use of the monthly mean zonal winds at Singapore at 30 hPa. The zonal wind data at 30 hPa were provided by the Freie Universität Berlin (FU-Berlin) at http://www.geo.fu-berlin.de/met/ag/strat/produkte/qbo/qbo.dat (last access: 15 June 2018) (Naujokat, 1986). The impact of ENSO in the tropics was investigated by using the Southern Oscillation Index (SOI) from the Bureau of Meteorology of the Australian Government (http://www.bom.gov.au/climate/current/soi2.shtml) (last access: 15 June 2018). The correlation between total ozone and the NAO index was mainly computed for the winter-mean (DJF) when the NAO amplitude is large (e.g. Hurrell and Deser, 2009), but it is also addressed in other seasons. Emphasis is given over Canada, Europe and the North Atlantic Ocean in winter. The principal component (PC)-based NAO index (DJF) provided by the Climate Analysis Section, NCAR, Boulder, USA (available at: https://climatedataguide.ucar.edu/climate-data/hurrell-north-atlantic-oscillation-nao-index-pc-based) (last access: 15 June 2018) was used. Total ozone variability is also related to dynamical variability, for example variability in tropopause height (e.g. Dameris et al., 1995; Hoinka et al., 1996; Steinbrecht et al., 1998). The impact of tropopause height variations on total ozone variability was examined by analyzing the tropopause pressure from the independently produced NCEP/NCAR (National Centers for Environmental Prediction/National Center for Atmospheric Research) reanalysis 1 data set computed on a 2.5^{o} grid. The NCEP/NCAR reanalysis data were provided from the web site at https://www.esrl.noaa.gov/psd/data/gridded/data.ncep.reanalysis.tropopause.html (last access: 15 June 2018) (Kalnay et al., 1996).

3 Results and discussion

3.1 Monthly zonal means and annual cycle

Figure 1 compares monthly mean total ozone from GOME-2A and SBUV (v8.6) satellite overpass data for stations shown in Table S1 (Supplement). The GOME-2A data were taken at a spatial resolution of 1^{o}x1^{o} around each of the ground-based monitoring stations listed in Supplement Table S1 and then averaged over the tropics, middle and high latitudes of both Hemispheres in 30^{o} latitudinal zones to provide the large scale monthly zonal means for the GOME-2A data. Accordingly, SBUV satellite overpass data were averaged over each geographical zone to provide the large scale zonal means for the SBUV observations. Mean differences and standard deviations between GOME-

2A and SBUV total ozone were found to be +0.1 ± 0.7% in the tropics (0-30 deg.), about +0.8 ± 1.6% in mid-latitudes (30-60 deg.), about +1.3 ± 2.2% over the northern high latitudes (60-80 deg. N) and about -0.5 ± 2.9% over the southern high latitudes (60-80 deg. S). The differences were estimated as [GOME-2A – SBUV] / SBUV (%) from January 2007 to December 2016. Small differences were also found between GOME-2A and GB measurements (Figure 2 and Table 1), where here GB stations data have been averaged over each geographical zone to provide the large scale zonal means for the GB measurements. Mean differences and standard deviations between GOME-2A and GB total ozone were found to be -0.7 ± 1.4% in the tropics (0-30 deg.), +0.1 ± 2.1% in mid-latitudes (30-60 deg.), +2.5 ± 3.2% over the northern high latitudes (60-80 deg. N) and 0.0 ± 4.3% over the southern high latitudes (60-80 deg. S). Recall that all estimates refer to the period between January 2007 and December 2016.

In summary, the largest differences between GOME-2A, SBUV (v8.6) and GB measurements are found over the northern high latitudes (60^o-80^o N) and the highest variability (standard deviation of the mean difference) is observed over the latitude belt (60^o-80^o S). In addition, these differences (especially at the high latitudes) can be affected by the fact that the same days have not always been used for the construction of the monthly mean values for the different datasets. In the tropics and mid-latitudes the respective differences are within ±1% or less, in line with Chiou et al. (2014). Validation results were also presented by Loyola et al. (2011), Koukouli et al. (2012), Coldewey-Egbers et al. (2015), Koukouli et al. (2015), updates of which are included in Hassinen et al. (2016). Our results based on data updated to 2017 largely confirm those studies, pointing to the good performance of GOME-2A when extending the period of record.

Next, we have studied the correlation between total ozone from GOME-2A and SBUV satellite data using linear regression analysis for the period 2007–2016. The statistical significance of the correlation coefficients, R, was calculated using the t-test formula for R with N-2 degrees of freedom, as used in Zerefos et al. (2018). The regression model showed statistically significant correlations between the different datasets as follows: R = +0.99 in the tropics, mid-latitudes and the northern high latitudes and R = +0.97 in the southern high latitudes. All correlation coefficients are highly statically significant (99.9% confidence level). In the long-term, statistically significant correlation coefficients ($R \geq +0.94$) are also found between GOME-2A satellite and GB measurements (Figure 2) despite the different type of instruments used to measure total ozone from the ground. The regression parameters for the correlation coefficients shown in Figures 1 and 2 are provided in Table 2.

A large part of the strong correlations shown in Figures 1 and 2 is attributable to the seasonal variability of total ozone which is presented in Figure 3 for GOME-2A, SBUV and GB data. More specifically, Figure 3 shows the seasonal variations of total ozone from station data, averaged per 10 degree latitude zones north and south. At high latitudes our analysis stops at 80 degrees. There is a very good agreement between the annual cycles of total ozone from the three datasets denoting the consistency of the satellite retrievals with GB observations. Similar annual cycles are also found with the GTO-ECV ozone data (not shown). Similar consistency is also revealed for the amplitudes of the annual cycles, computed as [(maximum value – minimum value)/2] in Dobson Units (DU). Figure 4 shows global maps of the amplitude of annual cycle of total ozone for the period 2007-2016 from GOME-2A (upper left panel), GTO-ECV (upper right) and the TOMS/OMI/OMPS (lower left) satellite data. All maps are

plotted against the sine of latitude north and south in order to show areas according to their actual size. As can be seen from Figure 4, the amplitude of annual cycle is less than 20 DU in the tropics, increasing as we move towards middle and high latitudes up to 75 DU. Interestingly, there is a region with small amplitude of annual cycle in the southern mid-latitudes with values of about 10-15 DU, seen in Figure 4 as a blue curved line crossing the longitudes around 60 degrees south, which points to small seasonal variations of total ozone in these parts. The seasonal increase in Antarctic ozone is delayed by 2-3 months compared to the north polar region. Only with the breakdown of the polar vortex in late spring, i.e. at a time when the poleward transport over lower latitudes has already ceased, does a strong ozone influx occur in the Antarctic. With this delay the amplitude of the seasonal variation stays much smaller poleward of 55-60^{o} in the south than in the north (Dütsch, 1974). These features are consistent between all examined satellite data sets and are reproduced to a large extend by the Oslo CTM3 model as well, except in the southern mid-latitudes where the model seems to underestimate the observed annual cycle (Figure 4 lower right).

In summary, we find a similar pattern and amplitude of annual cycle between total ozone from GOME-2A and the other examined total ozone data sets. The mean differences in the annual cycles of GOME-2A and SBUV satellite data are small in the tropics (0-30 deg.: 0.3 ± 2.4 DU), and increase as we move to mid-latitudes (30-60 deg.: 2.4 ± 4.4 DU) and higher latitudes (60-80 deg.: 1.7 ± 4.8 DU). These numbers are consistent with the ones found between GOME-2A and GB measurements (tropics: 1.1 ± 2.3 DU; mid-latitudes: 1.2 ± 5.1 DU; high latitudes: 5.1 ± 7.1 DU). In all latitude zones the correlation coefficients between the annual cycles of GOME-2A – SBUV and GOME-2A – GB data pairs were found to be greater than 0.9.

Before examining correlations with the large scale natural fluctuations QBO, ENSO and NAO, the mean annual cycle has been removed from the ozone data sets as described in the next section.

3.2 Correlation with QBO

We then studied how changes in dynamics affect the ozone columns in the atmosphere. The time series obtained have been deseasonalised by subtracting the long-term monthly mean from each individual monthly mean value. Ozone column variations for different latitude zones in the Northern and Southern Hemispheres have been compared. Figure 5 compares total ozone deseasonalised anomalies (in % of the mean) from GOME-2A and SBUV satellite retrievals in the tropics (10^{o} N–10^{o} S), sub-tropics (10^{o}–30^{o}) and mid-latitudes (30^{o}–60^{o}). The right panel of Figure 5 shows the respective anomalies from GTO-ECV data. Mean differences between GOME-2A and SBUV deseasonalised monthly zonal means between 60^{o} N and 60^{o} S are less than ±0.5%.

The line with dots superimposed on the ozone anomalies in Figure 5 shows the equatorial zonal winds at 30 hPa which were used as a proxy index to study the impact of QBO on total ozone. The general features include a QBO signal in total ozone at latitudes between 10^{o} N and 10^{o} S which almost matches with the phase of QBO in the zonal winds. At higher northern and southern latitudes there is a phase shift in the QBO impact on total ozone. The impact of QBO is most pronounced in the tropics and less pronounced in the sub-tropics and mid-latitudes. Strong positive correlations with the QBO are found in the tropics (correlation between GOME-2A and QBO of about +0.77, t-test = 12.91) and weaker (usually of opposite sign) less significant correlations are found at higher latitudes (about −0.15

in the northern and about −0.45 in the southern extra tropics). Similar correlation patterns with the QBO are found for the GTO-ECV, SBUV and GB data. These correlations suggest that the variability that can be attributed to the QBO in the tropics is about 60%, and about 2% and 20% in the northern and the southern extra tropics, respectively.

Table 3 summarizes the correlation and regression coefficients between total ozone and QBO at 30 hPa for the different latitude zones and the different datasets. For latitudes between 10^o N and 10^o S correlations between total ozone from GOME-2A, GTO-ECV, SBUV, GB data and the QBO are all positive. At latitudes between 10^o and 30^o the correlations turn to negative, in agreement with Knibbe et al. (2014) results, who noted that moving from the tropics towards higher latitudes the regression estimates switch to negative values at approximately 10^o N and 10^o S. The correlations with the QBO at 30 hPa remain negative up to 60^o, a consistent result among all our data sets, something also reported by Knibbe et al. (2014) with the MSR ozone data. The correlation and regression coefficients between GOME-2A and QBO are fairly similar to those found between SBUV and QBO, as well as among all data sets as seen in Table 3, despite the different periods of records.

These features are also evident in Figure 6 which compares GOME-2A (and GTO-ECV) satellite total ozone with GB observations with respect to the QBO. Mean differences and standard deviations between GOME-2A and GB and between GTO-ECV and GB deseasonalised total ozone data do not exceed one percent. Again, correlation coefficients between deseasonalised GOME-2A and deseasonalised GB data are highly significant in all latitude zones (30^o–60^o N: +0.91 (slope=0.818, error=0.035, t-value=23.466, N=119); 10^o–30^o N: +0.91 (slope=0.786, error=0.033, t-value=23.529, N=119; 10^o N–10^o S: +0.94 (slope=0.973, error=0.034, t-value=28.449, N=109; 10^o–30^o S: +0.87 (slope=0.864, error=0.044, t-value=19.659, N=119; 30^o–60^o S: +0.88 (slope=0.858, error=0.043, t-value=19.854, N=119). The same stands for the correlations between GTO-ECV and GB data pairs (30^o–60^o N: +0.94; 10^o–30^o N: +0.89; 10^o N–10^o S: +0.94; 10^o–30^o S: +0.87; 30^o–60^o S: +0.85). Our results are in line with Eleftheratos et al. (2013) and Isaksen et al. (2014) who compared QBO-related ozone column variations from the chemical transport model Oslo CTM2 with SBUV satellite data for shorter time periods. In summary, it has been shown that GOME-2A depicts the significant effects of QBO on stratospheric ozone in concurrence with SBUV and GB measurements. The instrument captures correctly the variability of ozone in the tropics and the mid-latitudes, which is nearly in phase with the QBO in the tropics and out of phase in the northern and the southern mid-latitudes as have been shown by earlier studies (e.g. Zerefos, 1983; Baldwin et al., 2001).

3.3 Correlation with ENSO

Apart from the QBO, which affects the variability of total ozone in the tropics, an important mode of natural climate variability in the tropics is ENSO. To examine the impact of ENSO on total ozone in the tropics we first removed variability related to the QBO and the solar cycle, and then performed the correlation analysis with the SOI. The effect of the QBO was removed from the time series by using a linear regression model for the total ozone variations at each grid box, of the form:

$$D(t) = a0 + a1 * QBO(t) + residuals(t); 0 < t \leq T \quad (1)$$

where D(t) is the monthly deseasonalised total ozone and t is the time in months with t=0 corresponding to the initial month and t=T corresponding to the last month. The term $a0$ is the intercept of the statistical model. To model QBO we made use of the equatorial zonal winds at 30 hPa. The term $a1$ is the regression coefficient of QBO. The QBO component was removed from the time series by using a phase lag with maximum correlation of 28 months (month lag -14 to month lag 13). The QBO-related coefficients $\alpha 0$ and $\alpha 1$ of Eq. (1) for the deseasonalized GOME-2A, GTO-ECV, TOMS/OMI/OMPS and Oslo CTM3 zonal mean data are presented in Table 3. Additional information for the regression coefficients $\alpha 1$ of QBO is provided in the Supplement Figure S1, which shows the spatial distribution of the regression coefficients in latitude-longitude maps.

The residuals from Eq. (1) were then inserted in a second regression (Eq. 2) to account for the effect of solar cycle on total ozone, as follows:

$$O_3(t) = \beta 0 + \beta 1 * F10.7(t) + residuals(t); 0 < t \leq T \quad (2)$$

where $\beta 0$ and $\beta 1$ are now the intercept and regression coefficients of solar cycle, respectively. To model the solar cycle we used the 10.7 cm wavelength solar radio flux (F10.7) as a proxy, taken from the National Research Council and Natural Resources Canada at ftp://ftp.geolab.nrcan.gc.ca/data/solar_flux/monthly_averages/solflux_monthly_average.txt (last access 12 December 2018). We use the absolute solar fluxes, which are adjusted to account for variations in Earth-Sun distance and uncertainty in antenna gain and waves reflected from the ground. Latitude-longitude maps of the regression coefficients $\beta 1$ of the solar cycle are presented in the Supplement Figure S2. We note that the global pattern of the regression coefficients of solar cycle from GOME-2A data matches well with what has been shown by Knibbe et al. (2014) with the reanalysis MSR data.

The remainders from Eq. (2) were used in a third regression (Eq. 3) to study the correlations between total ozone and SOI at each individual grid box:

$$O_3(t) = c0 + c1 * SOI(t) + residuals(t); 0 < t \leq T \quad (3)$$

where $c0$ and $c1$ are now the intercept and regression coefficients of ENSO, accordingly. Estimates of the regression coefficients $c1$ are shown in the Supplement Figure S3.

Figure 7 presents the correlations between SOI and total ozone from GOME-2A (upper left panel), GTO-ECV (upper right) and TOMS/OMI/OMPS satellite data (bottom left), as well as between SOI and the Oslo model simulations (bottom right). All four plots refer to the period 2007-2016. As can be seen from Figure 7 (upper left), correlations of >0.3 between GOME-2A total ozone and SOI are found in the tropical Pacific Ocean at latitudes between 25 deg. north and south. These correlations were tested as to their statistical significance in the period 2007-2016 using the t-test for R with N-2 degrees of freedom (as in Zerefos et al., 2018), and were found to be statistical significant. A similar picture of correlation coefficients is also observed by the GTO-ECV and TOMS/OMI/OMPS data. Both data sets show similar results as to the range of correlations (>0.3) in the tropical Pacific for the common period of observations. Nevertheless, the spatial resolution is higher in the GOME-2A and

GTO-ECV (1x1 deg.) data than in the TOMS/OMI/OMPS (5x5 deg.) data, so the former data sets perform better when looking at smaller space scales. We have to note here that in both maps there are larger areas with correlation coefficients >0.3 in the southern part of the tropics than in the northern part. However, this was mostly observed during the period 2007-2016. By examining the longer-term data record of the TOMS/OMI/OMPS data which extend back to 1979, we find symmetry in the pattern of correlations north and south of the equator in the tropical Pacific Ocean (Figure A1 of Appendix A), which indicates that both sides of the tropical Pacific are affected more or less in a similar way by El Niño/La Niña events. Finally, the Oslo CTM3 gives small correlations (<0.3) in the tropical Pacific Ocean around the equator, except over the northern and southern subtropics where the model compares better with the observations.

The small rectangle in Figure 7 corresponds to the South Pacific region (10^o-20^o S, 180^o-220^o E) and the blue cross to the station Samoa (American Samoa; 14.25^o S, 189.4^o E), at which total ozone has been studied as for the impact of ENSO after removing variability related to the annual cycle, QBO and the solar cycle. Figure 8 shows an example of the ENSO impact on total ozone in the South Pacific Ocean. The upper panel shows the time series of total ozone anomalies from GOME-2A, GTO-ECV and TOMS/OMI/OMPS satellite data together with the SOI (Figure 8a). Comparisons of GOME-2A data with GTO-ECV data, SBUV overpass data and GB measurements at the station Samoa are shown in Figure 8b. The dotted line shows the respective tropopause pressure anomalies from NCEP reanalysis. All data sets point to the strong influence of ENSO on total ozone. Most evident is the strong decrease of about 4% in 1997/98 which was caused by the strongest El Niño event in the examined period. A strong decrease is also observed in the tropopause pressures by NCEP. Notable also is the strong La Niña event in 2010 which caused total ozone to increase by about 4%. We calculate a strong correlation between total ozone from GTO-ECV and SOI of +0.66 (99% confidence level), which accounts for about 40% of the variability of total ozone over the tropical Pacific Ocean when the annual cycle, QBO signal and solar cycle are removed. From the regression with SOI we estimated an ENSO-related term from which we calculated the amplitude of ENSO in total ozone as [maximum ozone - minimum ozone]/2. The amplitude of ENSO in total ozone was estimated to be 8.8 DU or 3.5% of the annual mean. This is comparable to the amplitude of annual cycle (7.7 DU or 3.0% of the mean) and larger than the amplitude of QBO (2.2 DU or 0.8% of the mean) and the amplitude of solar cycle in this region (4.1 DU or 1.6% of the mean). These results are based on the GTO-ECV total ozone data. Similar results were also found at the station Samoa from GB observations (i.e. correlation with SOI: +0.55, amplitude of ENSO: 7.7 DU or 3.0% of the mean, amplitude of annual cycle: 6.7 DU or 2.7% of the mean). Statistics of total ozone such as mean, amplitude of annual cycle, amplitude of QBO, amplitude of solar cycle and amplitude of ENSO in total ozone over the selected areas are presented in Table 4. Both satellite, GB and model data show consistent results. It also appears that the station Samoa represents well the greater area in the Southern Pacific as to the impact of ENSO.

Differences between GOME-2A and its data pairs in the southern Pacific Ocean are the order of -0.2 ± 1.0% between GOME-2A and TOMS/OMI/OMPS data, -0.3 ± 0.9% between GOME-2A and GTO-ECV, and -0.9 ± 1.8% between GOME-2A and Oslo CTM3. Accordingly, differences at Samoa are: -0.6 ± 1.9% between GOME-2A and GB data, 0.0 ± 1.4% between GOME-2A and GTO-ECV, and -0.1 ± 1.3% between GOME-2A and SBUV. Despite the small differences found, we note here that GOME-2A values in the last 4 years of Figures 8 and 9 slightly

deviate from the other data sets, and correlate weaker with SOI than the other years in the time series. For instance, we estimate a drop in the correlation coefficient between GOME-2A and SOI at the station Samoa (+0.58 in the period 2007-2012 and +0.47 in the period 2007-2016), which nevertheless does not alter the statistical significance of the correlation.

From Figure 8 it also appears that there are high correlations with the tropopause height. The correlation coefficient between the NCEP tropopause pressure and GOME-2A total ozone over the South Pacific Ocean is of the order of +0.59 (Student's t-test statistics results: t-value = 7.946, p-value <0.0001, N = 119). Accordingly, the correlation with GTO-ECV ozone data is the order of +0.64 (t-value = 13.165, p-value <0.0001, N = 252) and with TOMS/OMI/OMPS the order of +0.58 (t-value = 10.913, p-value <0.0001, N = 241). The high correlation between the tropopause pressure and total ozone on interannual and longer time scales points to the very strong link between these parameters. These links were already documented in the past (e.g. Steinbrecht et al., 1998, 2001) and are verified with the GOME-2A data. At the same time a strong correlation is also evident between tropopause pressure and SOI, again on interannual and longer time scales (R= +0.66, t-value = 13.825, p-value <0.0001, N = 252). The above results point to the strong impact of ENSO on the tropical ozone column through the tropical tropopause; warm (El Niño) and cold (La Niña) events affect the variability of the tropopause which in turn affects the distribution of stratospheric ozone. In the tropics, where total ozone is mainly stratospheric, as the tropopause moves to higher altitudes (lower pressure), the stratosphere is compressed, reducing the amount of stratospheric (total) ozone. This happens during warm (El Niño) episodes. The opposite phenomenon occurs during cold (La Niña) events when the tropopause height decreases (higher pressure) and total ozone is then increased. These events can affect the long-term ozone trends in the tropics when looking at time periods when strong El Niño and La Niña events occur at the beginning and the end of the trend period respectively (Coldewey-Egbers et al., 2014).

Furthermore, in Figure 8 we have marked 7 stations in the greater South Asia region (35^o-45^o N, 45^o-125^o E) where total ozone is anti-correlated with the SOI. Admittedly, these anti-correlations are weak (about -0.3) but we thought worthwhile presenting the time series in these areas as well. Figure 9 shows the variability of total ozone after removing seasonal, QBO and solar cycle related variations, over the South Asia region (upper panel) and over the 7 stations averaged within this region (lower panel). As can be seen from this figure, the explained variance by ENSO is small, not exceeding 9%. All correlations from the comparisons with the SOI are summarized in Table 5. In spite the small correlations with the SOI, the consistency between GOME-2A, GTO-ECV, TOMS/OMI/OMPS and Oslo CTM3 data anomalies is very high and their differences are within ± 1%. Differences at the 7 stations in South Asia are as follows: -1.3 ± 2.4% between GOME-2A and GB data, -0.4 ± 1.0% between GOME-2A, and GTO-ECV and -0.5 ± 1.0% between GOME-2A and SBUV.

In summary, our findings indicate that GOME-2A captures well the disturbances in total ozone during ENSO events with respect to satellite SBUV and GB observations. Our findings on the ENSO-related total ozone variations (low ozone during ENSO warm events, high ozone during ENSO cold events, and magnitude of changes) are in line with recent studies (e.g. Randel and Thompson, 2011; Oman et al., 2013, Sioris et al., 2014) included in the 2014 Ozone

Assessment report (Pawson et al., 2014; WMO, 2014). Our results are also in agreement with Knibbe et al. (2014) who showed negative ozone effects of El Niño between 25° S and 25° N, especially over the Pacific.

3.4 Correlation with NAO

The residuals from Eq. (3), free from seasonal, QBO, solar and ENSO related variations, were later used to study the correlation between total ozone and NAO in winter. The results are presented in Figure 10 which shows the correlation coefficients between total ozone and NAO index in winter from the GOME-2A (upper left), GTO-ECV (upper right) and TOMS/OMI/OMPS satellite data (lower left), and the Oslo CTM3 model calculations (lower right). Negative correlations between total ozone and NAO are presented with blue colours while positive correlations with red colours. From Figure 10 (upper left) it appears that total ozone is strongly correlated with NAO in many regions. Strong negative correlation coefficients are observed in the majority of the northern mid-latitudes (R about −0.6) while positive correlations exist in the tropics and some negative correlations in the southern mid-latitudes. These characteristics are observed in both GTO-ECV and TOMS/OMI/OMPS datasets and are reproduced by the Oslo model as well, all for the common period 2007-2016. The regression coefficients on these comparisons are presented in the Supplement Figure S4.

We note here that the results of the correlation analysis for the period 2007-2016 were based on a relative small sample of data from 10 winters and therefore many of these correlation coefficients may not be statistically significant. The statistical significance of the correlation coefficients in every grid box was tested only with the TOMS/OMI/OMPS data (Figure A2, Appendix A), which provided us the opportunity to calculate the respective correlations using data for the whole period of record 1979-2016. It appears that when extending the data back to the 1980's the negative correlations in the southern mid-latitudes in winter disappear while the positive correlations in the tropics become weaker; yet the observed anti-correlation between total ozone and NAO index in the northern mid-latitude zone holds strong. The dotted line in the plot shows areas with statistically significant correlation coefficients (99% confidence level). Indeed, in the long-term, statistically significant correlations between total ozone and the NAO index during winter are mostly found over the northern mid-latitudes and the sub-tropics. A small, statistically significant signal is also seen over Antarctica but it was not analysed further.

According to this finding we have restricted the analysis of NAO to the northern mid-latitudes. Rectangles (Figure 10, upper left) correspond to two regions in the North Atlantic, i.e., 35°-50° N, 20°-50° W and 15°-27° N, 30°-60° W respectively, which were studied for the impact of NAO on total ozone after removing variability related to the annual cycle, QBO, solar cycle and ENSO. In addition we have studied a number of stations in Canada, USA, and Europe contributing ozone data to WOUDC, which are marked by red and green crosses in Figure 10. The red crosses refer to the monitoring stations in Canada and the US, and the green crosses to the stations in Europe. In Figure 11 we present the times series of total ozone anomalies from GOME-2A, GTO-ECV and TOMS/OMI/OMPS satellite data along with the NAO index in winter over the North Atlantic. Model calculations are shown as well. The dotted line shows the respective tropopause pressure anomalies from NCEP reanalysis. Comparisons between GOME-2A, GTO-ECV, SBUV (v8.6) overpass data and GB measurements over the various stations in Canada, USA and Europe are shown in Figure 12.

The observed anomalies over the North Atlantic Ocean point to the strong influence of NAO on total ozone in winter. Most evident is the strong increase in total ozone in 2010 of more than 8% particularly over 35^o-50^o N and 20^o-50^o W. This increase was accompanied by a strong increase in tropopause pressures. Both changes (in total ozone and tropopause pressures) occurred under a strong negative phase of NAO, the strongest one in the past 20 years. We observe strong anti-correlation among total ozone and NAO index in winter (R= –0.74 over 35^o-50^o N, 20^o-50^o W), which is statistically significant at the 99% confidence level. This anti-correlation suggests that about 50% of the variability of total ozone in winter is explained by NAO when the annual cycle, QBO, solar cycle and ENSO signals are removed. Differences for GOME-2A and its data pairs are estimated to be -0.7 ± 1.1% between GOME-2A and TOMS/OMI/OMPS data, +0.1 ± 1.0% between GOME-2A and GTO-ECV, and -0.2 ± 1.5% between GOME-2A and Oslo CTM3. From the regression with the NAO index we derived a NAO-related term from which we calculated the amplitude of NAO in total ozone as [maximum ozone - minimum ozone]/2. The amplitude of NAO over the North Atlantic region (35^o-50^o N, 20^o-50^o W) was estimated to be about 16.5 DU or 5.2% of the annual mean. This is about half of the amplitude of the annual cycle (which is ~37 DU or 11.7% of the mean). These estimates are based on GTO-ECV data. Similar correlation and amplitude were also found with GOME-2A, the combined TOMS/OMI/OMPS satellite data and the Oslo CTM3 model simulations.

A similar but opposite correlation is found over the southern part of the North Atlantic (15^o-27^o N, 30^o-60^o W). Here, we estimate a significant correlation coefficient with NAO of +0.60, amplitude of NAO of about 7.2 DU (2.6% of the annual mean) and amplitude of annual cycle of about 15.8 DU (5.7% of the mean). Again, similar estimates are found with the GOME-2A and the TOMS/OMI/OMPS satellite data and reproduced by the model calculations as well. The annual mean total ozone and the amplitudes of annual cycle, QBO, solar cycle and NAO in total ozone over the studied regions in the North Atlantic are summarised in Table 6. Differences between GOME-2A and GTO-ECV data at the southern part of North Atlantic are the order of -0.6 ± 0.7%. Differences with the TOMS/OMI/OMPS data are estimated to be -0.9 ± 0.8%, and with the Oslo CTM3 -0.1 ± 0.7%.

The time series of total ozone anomalies and of the NAO index for the examined stations in Canada, USA and Europe are presented in Figure 12. Table 7 presents the respective statistics. The correlation between total ozone and the NAO index in winter after removing from ozone variability related to the annual cycle, QBO, solar cycle and ENSO is –0.40 (90% confidence level). Again, a particular feature was the total ozone increase in 2010 by 6% of the mean associated with the negative NAO phase. Noteworthy on this increase is the consistency with the GB measurements and the satellite SBUV overpass data, and in general the agreement found between the variability of the tropopause pressures and total ozone. Differences between GOME-2A and GB data are -1.0 ± 1.8%. Accordingly we estimate differences of about -1.1 ± 0.5% between GOME-2A and GTO-ECV data and of about -1.3 ± 0.6% between GOME-2A and SBUV data. On the basis of GTO-ECV data we estimate that in Canada and USA, the amplitude of NAO in total ozone in winter is about 7 DU (or 2.2% of the mean), while it is estimated to be about 9 DU (or 2.7% of the mean) over Europe. These numbers are slightly smaller than the GOME-2A, GB and SBUV estimates, less than about one percent (Table 7).

The anti-correlation between total ozone column and the NAO index during winter also applies to southern Europe and the Mediterranean. Following the study of Ossó et al. (2011) who reported a reversal in the correlation pattern between NAO and total ozone from winter to summer in southern Europe, we have looked at the correlations during summer as well. Figure 13 presents the comparisons for 21 ground-based stations located in the region bounded by latitudes 30^{o}-47^{o} N and by longitudes 10^{o}W-40^{o}E. Figure 13a shows results for the summer and Figure 13b shows results for winter. As evident, the observed anti-correlation between GB total ozone and NAO in winter (R= -0.43, slope= -0.980, t-value= -2.095, p-value= 0.0499, N = 21) reverses sign and becomes positive in the summer (R= +0.60, slope= 0.874, t-value= 3.309, p-value= 0.0037, N= 21), indicating that the NAO explains about 36% of ozone variability in the summer in this region. A similar picture is also seen from GOME-2A, GTO-ECV and SBUV data.

In summary, our findings based on GOME-2A, GTO-ECV and SBUV overpass data are in line with those found by Ossó et al. (2011) and Steinbrecht et al. (2011) who analysed TOMS and OMI satellite data, and GB measurements at the station Hohenpeissenberg, respectively. During winter, total ozone variability associated with the NAO is particularly important over northern Europe, the U.S. East Coast, and Canada, explaining up to 30% in total ozone variance for this region (Ossó et al., 2011). Also, both studies found unusually high total ozone columns in 2010 over much of the Northern Hemisphere and related them to the negative phase of NAO or AO (the Arctic Oscillation).

4 Conclusions

We have evaluated the ability of GOME-2/MetopA (GOME-2A) satellite total ozone retrievals to capture known natural oscillations such as the QBO, ENSO and NAO. In general, GOME-2A depicts these natural oscillations in concurrence with GTO-ECV, TOMS/OMI/OMPS, SBUV (v8.6) satellite overpass data, ground-based measurements (Brewer, Dobson, filter and SAOZ) and chemical transport model calculations (Oslo CTM3).

Mean differences between GOME-2A and SBUV total ozone were found to be +0.1 ± 0.7% in the tropics (0-30 deg.), about +0.8 ± 1.6% in mid-latitudes (30-60 deg.), about +1.3 ± 2.2% over the northern high latitudes (60-80 deg. N) and about -0.5 ± 2.9% over the southern high latitudes (60-80 deg. S). These differences were estimated as [GOME-2A – SBUV] / SBUV (%) from January 2007 to December 2016. Small differences were also found between GOME-2A and GB measurements, with standard deviations of the differences being ± 1.4% in the tropics, ± 2.1% in mid-latitudes, and ± 3.2% and ± 4.3% over the northern and the southern high latitudes respectively.

The variability of total ozone from GOME-2A has been compared with the variability of total ozone from other examined data sets as to their agreement depicting natural atmospheric phenomena such as the QBO, ENSO and NAO. First, we studied correlations between total ozone and the QBO after removing from the ozone data sets variability related to the seasonal cycle. Then, we examined correlations between total ozone and ENSO, after removing variability related to the QBO and solar cycle, and finally correlations with the NAO after removing variability related to the QBO, solar cycle and ENSO. Our main results are as follows:

QBO: Total ozone from GOME-2A is well correlated with the Quasi-Biennial Oscillation (+0.8 in the tropics) in agreement with GTO-ECV, SBUV and GB data. The amplitude of QBO on total ozone maximizes around the equator and it is estimated to about 2.6% of the mean. Going from low to mid-latitudes there is a phase shift in the QBO impact on total ozone. Correlation coefficients between GOME-2A total ozone and the QBO over 30-60 deg. north and south are -0.1 and -0.5 respectively, in agreement with the correlations between GB total ozone and the QBO (-0.2 and -0.5, accordingly). On the basis of GOME-2A, the amplitude of QBO in total ozone is estimated to be 0.6% of the mean in the northern mid-latitudes and 1.4% of the mean in the southern mid-latitudes.

ENSO: Correlation coefficients among GOME-2A total ozone and SOI in the tropical Pacific Ocean are estimated to be about +0.6, consistent with GTO-ECV, SBUV and GB observations. It was found that the El Nino Southern Oscillation (ENSO) signal is evident and consistent in all examined datasets. The amplitude of ENSO in total ozone is about 6–9 DU corresponding to about 2.5–3.5% of the annual mean. Differences between GOME-2A, GTO-ECV and GB measurements during warm (El Niño) and cold (La Niña) events are within ±1.5%. Similar estimates also result from the Dobson measurements at American Samoa, indicating that Samoa station represents well the greater area in the Southern Pacific for satellite evaluations as to the impact of ENSO.

NAO: The respective results as far as the impact of the North Atlantic Oscillation over the northern mid-latitudes showed a clear NAO signal in winter in all data sets, with amplitudes of about 16-19 DU (about 5–6% of the annual mean) in the North Atlantic, 9-12 DU (3-4% of the mean) over Europe, and 7-10 DU (2-3% of the mean) over Canada and the US. Comparison with GB observations over Canada and Europe showed very good agreement between GOME-2A, GTO-ECV and GB observations as to the influence by NAO, with differences within ±1%.

In addition to the usual validation methods, which compare monthly mean and zonal mean total ozone data and analyse the differences between satellite and GB instruments, we showed here that quasi cyclical perturbations such as the QBO, ENSO and NAO can serve as independent proxies of spatiotemporal variation to qualitatively evaluate GOME-2A satellite total ozone against ground-based and other satellite total ozone data sets. The agreement and small differences which were found between the variability of total ozone from GOME-2A and the variability of total ozone from other satellite retrievals and ground-based measurements during these naturally-occurring oscillations verify the good quality of GOME-2A satellite total ozone to be used in ozone-climate research studies.

Data availability

Satellite SBUV (v8.6) total ozone station overpass data were downloaded from https://acd-ext.gsfc.nasa.gov/Data_services/merged/index.html (last access: 15 June 2018) (McPeters et al., 2013; Bhartia et al., 2013). GTO-ECV total ozone data are available at http://www.esa-ozone-cci.org/?q=node/160 (last access: 15 June 2018) (Coldewey-Egbers et al., 2015; Garane et al., 2018). Ground-based total ozone daily summaries were obtained from the World Ozone and UV Data Centre (WOUDC) at https://woudc.org/archive/Summaries/TotalOzone/Daily_Summary/ (last access: 15 June 2018). The QBO component on total ozone was examined by using the monthly mean zonal winds at Singapore at 30 hPa. Zonal

wind data at 30 hPa were provided by the Freie Universität Berlin (FU-Berlin) at http://www.geo.fu-berlin.de/met/ag/strat/produkte/qbo/qbo.dat (last access: 15 June 2018) (Naujokat, 1986). The Southern Oscillation Index (SOI) was provided by the Bureau of Meteorology of the Australian Government at http://www.bom.gov.au/climate/current/soi2.shtml (Australian Government – Bureau of Meteorology, 2018). The NAO index for December, January and February was provided by the Climate Analysis Section, NCAR, Boulder, USA at https://climatedataguide.ucar.edu/climate-data/hurrell-north-atlantic-oscillation-nao-index-pc-based (last access: 15 June 2018) (Hurrell and Deser, 2009). The tropopause pressures from the NCEP/NCAR reanalysis 1 data set were downloaded from https://www.esrl.noaa.gov/psd/data/gridded/data.ncep.reanalysis.tropopause.html (last access: 15 June 2018) (Kalnay et al., 1996).

Competing interests

The authors declare that they have no conflict of interest.

Acknowledgements

Development of the GOME-2/MetopA total ozone products and their validation has been funded by the AC SAF project with EUMETSAT and national contributions. We further acknowledge the Mariolopoulos-Kanaginis Foundation for the Environmental Sciences, the ESA Ozone CCI project and the NASA Goddard Space Flight Centre. The ground-based data used in this publication were obtained as part of WMO's Global Atmosphere Watch (GAW) and are publicly available via the World Ozone and UV Data Centre (WOUDC). The authors would like to thank all the investigators that provide quality assured total ozone column data on a timely basis to the WOUDC database. We acknowledge the National Oceanic and Atmospheric Administration (NOAA) for maintaining the American Samoa Dobson station. KE and CS would like to dedicate the study to the memory of Professor Ivar Isaksen (University of Oslo) who passed away on May 16th, 2017.

References

Australian Government – Bureau of Meteorology: Southern Oscillation Index (SOI) since 1986, available at http://www.bom.gov.au/climate/current/soi2.shtml, last access: 15 June 2018.

Baldwin, M. P., Gray, L. J., Dunkerton, T. J., Hamilton, K., Haynes, P. H., Randel, W. J., Holton, J. R., Alexander, M. J., Hirota, I., Horinouchi, T., Jones, D. B. A., Kinnersley, J. S., Marquardt, C., Sato, K., and Takahashi, M.: The quasi-biennial oscillation, Rev. Geophys., 39, 179-229, doi: 10.1029/1999RG000073, 2001.

Bhartia, P. K., McPeters, R. D., Flynn, L. E., Taylor, S., Kramarova, N. A., Frith, S., Fisher, B., and DeLand, M.: Solar Backscatter UV (SBUV) total ozone and profile algorithm, Atmos. Meas. Tech., 6, 2533–2548, doi: 10.5194/amt-6-2533-2013, 2013.

Brönnimann, S., Bhend, J., Franke, J., Flückiger, S., Fischer, A. M., Bleisch, R., Bodeker, G., Hassler, B., Rozanov, E., and Schraner, M.: A global historical ozone data set and prominent features of stratospheric variability prior to 1979, Atmos. Chem. Phys., 13 (18), 9623-9639, doi: 10.5194/acp-13-9623-2013, 2013.

Chehade, W., Weber, M., and Burrows, J. P.: Total ozone trends and variability during 1979-2012 from merged data sets of various satellites, Atmos. Chem. Phys., 14, 7059–7074, doi: 10.5194/acp-14-7059-2014, 2014.

Chiou, E. W., Bhartia, P. K., McPeters, R. D., Loyola, D. G., Coldewey-Egbers, M., Fioletov, V. E., Van Roozendael, M., Spurr, R., Lerot, C., and Frith, S. M.: Comparison of profile total ozone from SBUV (v8.6) with GOME-type and ground-based total ozone for a 16-year period (1996 to 2011), Atmos. Meas. Tech., 7, 1681–1692, doi: 10.5194/amt-7-1681-2014, 2014.

Coldewey-Egbers, M., Loyola R., D. G., Braesicke, P., Dameris, M., van Roozendael, M., Lerot, C., and W. Zimmer, W.: A new health check of the ozone layer at global and regional scales, Geophys. Res. Lett., 41, 4363–4372, doi:10.1002/2014GL060212, 2014.

Coldewey-Egbers, M., Loyola, D. G., Koukouli, M., Balis, D., Lambert, J.-C., Verhoelst, T., Granville, J., van Roozendael, M., Lerot, C., Spurr, R., Frith, S. M., and Zehner, C.: The GOME-type Total Ozone Essential Climate Variable (GTO-ECV) data record from the ESA Climate Change Initiative, Atmos. Meas. Tech., 8, 3923–3940, doi: 10.5194/amt-8-3923-2015, 2015.

Dameris, M., Nodorp, D., and Sausen, R.: Correlation between Tropopause Height Pressure and TOMS-Data for the EASOE-Winter 1991/1992, Beitr. Phys. Atmosph., 68 (3), 227-232, 1995.

de Laat, A. T. J., van Weele, M., and van der A., R. J.: Onset of stratospheric ozone recovery in the Antarctic ozone hole in assimilated daily total ozone columns, Journal of Geophysical Research: Atmospheres, 122, 11880-11899, https://doi.org/10.1002/2016JD025723, 2017.

Dütsch, H. U.: The ozone distribution in the atmosphere, Can. J. Chem, 52, 1491-1504, 1974.

Eleftheratos, K., Isaksen, I., Zerefos, C., Nastos, P., Tourpali, K., and Rognerud, B.: Ozone variations derived by a chemical transport model, Water, Air and Soil Pollution, 224:1585, doi: 10.1007/s11270-013-1585-2, 2013.

Eleftheratos, K., Isaksen, I. S. A., Zerefos, C. S., Tourpali, K., and Nastos, P.: Comparison of Ozone Variations from Model Calculations (OsloCTM2) and Satellite Retrievals (SBUV), 11th International Conference on Meteorology, Climatology and Atmospheric Physics (COMECAP 2012), Athens, Greece, 29 May – 1 June 2012, C. G. Helmis and P. T. Nastos (eds.), Advances in Meteorology, Climatology and Atmospheric Physics, Springer Atmospheric Sciences, DOI 10.1007/978-3-642-29172-2_132, © Springer-Verlag Berlin Heidelberg, pp. 945–950, 2012.

Frith, S. M., Kramarova, N. A., Stolarski, R. S., McPeters, R. D., Bhartia, P. K., and Labow, G. J.: Recent changes in total column ozone based on the SBUV Version 8.6 merged ozone data set, J. Geophys. Res., 119, 9735–9751, doi: 10.1002/2014JD021889, 2014.

Frossard, L., Rieder, H. E., Ribatet, M., Staehelin, J., Maeder, J. A., Di Rocco, S., Davison, A. C., and Peter, T.: On the relationship between total ozone and atmospheric dynamics and chemistry at mid-latitudes – Part 1: Statistical

631 models and spatial fingerprints of atmospheric dynamics and chemistry, Atmos. Chem. Phys., 13 (1), 147-164, doi:
632 10.5194/acp-13-147-2013, 2013.

633 Garane, K., Lerot, C., Coldewey-Egbers, M., Verhoelst, T., Koukouli, M. E., Zyrichidou, I., Balis, D. S., Danckaert,
634 T., Goutail, F., Granville, J., Hubert, D., Keppens, A., Lambert, J.-C., Loyola, D., Pommereau, J.-P., Van
635 Roozendael, M., and Zehner, C.: Quality assessment of the Ozone_cci Climate Research Data Package (release
636 2017) – Part 1: Ground-based validation of total ozone column data products, Atmos. Meas. Tech., 11, 1385-1402,
637 doi:10.5194/amt-11-1385-2018, 2018.

638 Hao, N., Koukouli, M. E., Inness, A., Valks, P., Loyola, D. G., Zimmer, W., Balis, D. S., Zyrichidou, I., Van
639 Roozendael, M., Lerot, C., and Spurr, R. J. D.: GOME-2 total ozone columns from MetOp-A/MetOp-B and
640 assimilation in the MACC system, Atmos. Meas. Tech., 7, 2937–2951, doi: 10.5194/amt-7-2937-2014, 2014.

641 Hassinen, S., Balis, D., Bauer, H., Begoin, M., Delcloo, A., Eleftheratos, K., Gimeno Garcia, S., Granville, J.,
642 Grossi, M., Hao, N., Hedelt, P., Hendrick, F., Hess, M., Heue, K.-P., Hovila, J., Jønch-Sørensen, H., Kalakoski, N.,
643 Kauppi, A., Kiemle, S., Kins, L., Koukouli, M. E., Kujanpää, J., Lambert, J.-C., Lang, R., Lerot, C., Loyola, D.,
644 Pedergnana, M., Pinardi, G., Romahn, F., van Roozendael, M., Lutz, R., De Smedt, I., Stammes, P., Steinbrecht, W.,
645 Tamminen, J., Theys, N., Tilstra, L. G., Tuinder, O. N. E., Valks, P., Zerefos, C., Zimmer, W., and Zyrichidou, I.:
646 Overview of the O3M SAF GOME-2 operational atmospheric composition and UV radiation data products and data
647 availability, Atmos. Meas. Tech., 9, 383–407, doi: 10.5194/amt-9-383-2016, 2016.

648 Hegglin, M. I., Fahey, D. W., McFarland, M., Montzka, S. A., and Nash, E. R.: Twenty questions and answers about
649 the ozone layer: 2014 update, Scientific Assessment of Ozone Depletion: 2014, 84 pp., World Meteorological
650 Organization, Geneva, Switzerland, ISBN: 978-9966-076-02-1, 2015.

651 Hoinka, K. P., Claude, H., and Köhler, U.: On the correlation between tropopause pressure and ozone above Central
652 Europe, Geophys. Res. Lett., 23 (14), 1753-1756, 1996.

653 Hurrell, J. W., and Deser, C.: North Atlantic climate variability: The role of the North Atlantic Oscillation, Journal
654 of Marine Systems, 78, 28-41, doi: 10.1016/j.jmarsys.2008.11.026, 2009.

655 Isaksen, I. S. A., Berntsen, T. K., Dalsøren, S. B., Eleftheratos, K., Orsolini, Y., Rognerud, B., Stordal, F., Søvde, O.
656 A., Zerefos, C., and Holmes, C. D.: Atmospheric ozone and methane in a changing climate, Atmosphere, 5, 518–
657 535, doi: 10.3390/atmos5030518, 2014.

658 Kalnay, E., Kanamitsu, M., Kistler, R., Collins, W., Deaven, D., Gandin, L., Iredell, M., Saha, S., White, G.,
659 Woollen, J., Zhu, Y., Chelliah, M., Ebisuzaki, W., Higgins, W., Janowiak, J., Mo, K. C., Ropelewski, C., Wang, J.,
660 Leetmaa, A., Reynolds, R., Jenne, R., and Joseph, D.: The NCEP/NCAR 40-year reanalysis project, Bulletin of the
661 American Meteorological Society, Vol. 77, No. 3, 437-472, 1996.

662 Knibbe, J. S., van der A, R. J., and de Laat, A. T. J.: Spatial regression analysis on 32 years of total column ozone
663 data, Atmos. Chem. Phys., 14, 8461-8482, https://doi.org/10.5194/acp-14-8461-2014, 2014.

Koukouli, M. E., Balis, D. S., Loyola, D., Valks, P., Zimmer, W., Hao, N., Lambert, J.-C., Van Roozendael, M., Lerot, C., and Spurr, R. J. D.: Geophysical validation and long-term consistency between GOME-2/MetOp-A total ozone column and measurements from the sensors GOME/ERS-2, SCIAMACHY/ENVISAT and OMI/Aura, Atmos. Meas. Tech., 5, 2169–2181, doi: 10.5194/amt-5-2169-2012, 2012.

Koukouli, M. E., Lerot, C., Granville, J., Goutail, F., Lambert, J-C., Pommereau, J-P., Balis, D., Zyrichidou, I., Van Roozendael, M., Coldewey-Egbers, M., Loyola, D., Labow, G., Frith, S., Spurr, R., Zehner, C.: Evaluating a new homogeneous total ozone climate data record from GOME/ERS-2, SCIAMACHY/Envisat and GOME-2/MetOp-A, J. Geophys. Res. Atmos., 120, doi: 10.1002/2015JD023699, 2015.

Kuttippurath, J. and Nair, P. J.: The signs of Antarctic ozone hole recovery, Sci. Rep., 7, https://doi.org/10.1038/s41598-017-00722-7, 2017.

Labow, G. J., McPeters, R. D., Bhartia, P. K., and Kramarova, N.: A comparison of 40 years of SBUV measurements of column ozone with data from the Dobson/Brewer network, J. Geophys. Res. Atmos., 118, 7370-7378, doi:10.1002/jgrd.50503, 2013.

Lerot, C., Van Roozendael, M., Spurr, R., Loyola, D., Coldewey-Egbers, M. Kochenova, S., van Gent, J., Koukouli, M., Balis, D., Lambert, J.-C., Granville, J., and Zehner, C.: Homogenized total ozone data records from the European sensors GOME/ERS-2, SCIAMACHY/Envisat, and GOME-2/MetOp-A, J. Geophys. Res. Atmos., 119, 1639–1662, doi: 10.1002/2013JD020831, 2014.

Loyola, D. G., Koukouli, M. E., Valks, P., Balis, D. S., Hao, N., Van Roozendael, M., Spurr, R. J. D., Zimmer, W., Kiemle, S., Lerot, C., and Lambert, J.-C.: The GOME-2 total column ozone product: retrieval algorithm and ground-based validation, J. Geophys. Res., 116, D07302, doi: 10.1029/2010JD014675, 2011.

McPeters, R. D., Bhartia, P. K., Haffner, D., Labow, G. J., and Flynn, L.: The version 8.6 SBUV ozone data record: An overview, J. Geophys. Res., 118, 8032–8039, doi: 10.1002/jgrd.50597, 2013.

McPeters, R. D., Frith, S, and Labow, G. J.: OMI total column ozone: extending the long-term data record, Atmos. Meas. Tech., 8, 4845-4850, soi:10.5194/amt-8-4845-2015, 2015.

Naujokat, B., 1986: An update of the observed quasi-biennial oscillation of the stratospheric winds over the tropics, J. Atmos. Sci., 43, 1873-1877.

Oman, L., Douglass, A., Ziemke, J., Rodriguez, J., Waugh, D., and Nielsen, J.: The ozone response to ENSO in Aura satellite measurements and a chemistry-climate simulation, J. Geophys. Res., 118 (2), 965-976, doi: 10.1029/2012JD018546, 2013.

Ossó, A., Sola, Y., Bech, J., and Lorente, J.: Evidence for the influence of the North Atlantic Oscillation on the total ozone column at northern low latitudes and midlatitudes during winter and summer seasons, J. Geophys. Res., 116 (D24), D24122, doi: 10.1029/2011JD016539, 2011.

Pawson, S., and Steinbrecht, W. (Lead Authors), Charlton-Perez, A. J., Fujiwara, M., Karpechko, A. Yu., Petropavlovskikh, I., Urban, J., and Weber, M.: Update on global ozone: Past, present, and future, V. E. Violetov

and U. Langematz (Eds), Chapter 2 in Scientific Assessment of Ozone Depletion: 2014, Global Ozone Research and Monitoring Project – Report No. 55, World Meteorological Organization, Geneva, Switzerland, 2014.

Pazmiño, A., Godin-beekmann, S., Hauchecorne, A., Claud, C., Khaykin, S., Goutail, F., Wolfram, E., Salvador, J., and Quel, E.: Multiplesymptoms of total ozone recovery inside the Antarctic vortex during austral spring, Atmos. Chem. Phys, 18, 7557–7572, 2018.

Prather, M.: Fast-JX version 6.7c, available at: ftp://halo.ess.uci.edu/public/prather/Fast-J/ (last access: 15 June 2018), 2012.

Randel, W. J., and Thompson, A. M.: Interannual variability and trends in tropical ozone derived from SAGE II satellite data and SHADOZ ozonesondes, J. Geophys. Res., 116 (D7), D07303, doi: 10.1029/2010JD015195, 2011.

Rieder, H. E., Frossard, L., Ribatet, M., Staehelin, J., Maeder, J. A., Di Rocco, S., Davison, A. C., Peter, T., Weihs, P., and Holawe, F.: On the relationship between total ozone and atmospheric dynamics and chemistry at midlatitudes – Part 2: The effects of the El Niño/Southern Oscillation, volcanic eruptions and contributions of atmospheric dynamics and chemistry to long-term total ozone changes, Atmos. Chem. Phys., 13 (1), 165-179, doi: 10.5194/acp-13-165-2013, 2013.

Sander, S. P., Abbatt, J., Barker, J. R., Burkholder, J. B., Friedl, R. R., Golden, D. M., Huie, R. E., Kolb, C. E., Kurylo, M. J., Moortgat, G. K., Orkin V. L., and Wine, P. H.: Chemical Kinetics and Photochemical Data for Use in Atmospheric Studies, Evaluation No. 17, JPL Publication 10-6, Jet Propulsion Laboratory, Pasadena, 2011, (http://jpldataeval.jpl.nasa.gov; last access 15 June 2018), 2011.

Sioris, C. E., McLinden, C. A., Fioletov, V. E., Adams, C., Zawodny, J. M.m Bourassa, A. E., Roth, C. Z., and Degenstein, D. A.: Trend and variability in ozone in the tropical lower stratosphere over 2.5 solar cycles observed by SAGE II and OSIRIS, Atmos. Chem. Phys., 14, 3479-3496, doi: 10.5194/acp-14-3479-2014, 2014.

Søvde, O. A., Prather, M. J., Isaksen, I. S. A., Berntsen, T. K., Stordal, F., Zhu, X., Holmes, C. D., and Hsu, J.: The chemical transport model Oslo CTM3, Geosci. Model Dev., 5, 1441–1469, doi: 10.5194/gmd-5-1441-2012, 2012.

Solomon, S., Ivy, D. J., Kinnison, D., Mills, M. J., Neely III, R. R., and Schmidt, A.: Emergence of healing in the Antarctic ozone layer, Science, 30, doi: 10.1126/science.aae0061, 2016.

Steinbrecht, W., Claude, H., Köhler, U., and Hoinka, K. P.: Correlations between tropopause height and total ozone: Implications for long-term changes, J. Geophys. Res., 103 (D15), 19183-19192, 1998.

Steinbrecht, W., Claude, H., Köhler, U., and Winkler, P.: Interannual changes of total ozone and Northern Hemisphere circulation patterns, Geophys. Res. Lett., 28, 1191-1194, 2001.

Steinbrecht, W., Köhler, U., Claude, H., Weber, M., Burrows, J. P., and van der A, R. J.: Very high ozone columns at northern mid-latitudes in 2010, Geophys. Res. Lett., 38 (6), L06803, doi: 10.1029/2010GL046634, 2011.

Stone, K. A., Solomon, S., and Kinnison, D. E.: On the identification of ozone recovery, Geophysical Research Letters, 45, 5158-5165, https://doi.org/10.1029/2018GL077955, 2018.

Strahan, S. E. and Douglass, A. R.: Decline in Antarctic Ozone Depletion and Lower Stratospheric Chlorine Determined From Aura Microwave Limb Sounder Observations, Geophys. Res. Lett., 45, 382–390, https://doi.org/10.1002/2017GL074830, 2018.

Tourpali, K., Zerefos, C. S., Balis, D. S., and Bais, A. F.: The 11-year solar cycle in stratospheric ozone: Comparison between Umkehr and SBUVv8 and effects on surface erythemal irradiance, J. Geophys. Res., 112 (D12), D12306, doi: 10.1029/2006JD007760, 2007.

Van Roozendael, M., Spurr, R. J. D., Loyola, D., Lerot, C., Balis, D. S., Lambert, J.C., Zimmer, W., van Gent, J., van Geffen, J., Koukouli, M., Doicu, A., and Zehner, C.: Sixteen years of GOME/ERS-2 total ozone data: The new direct-fitting GOME Data Processor (GDP) version 5 – Algorithm description, J. Geophys Res., 117, D03305, doi: 10.1029/2011JD016471, 2012.

WMO (World Meteorological Organization), *Scientific Assessment of Ozone Depletion: 2014*, Global Ozone Research and Monitoring Project–Report No. 55, 416 pp., Geneva, Switzerland, 2014.

Zerefos, C. S.: On the quasi-biennial oscillation in stratospheric temperatures and total ozone, Advances in Space Research, 2, 177–181, 1983.

Zerefos, C. S., Bais, A. F., and Ziomas, I. C.: On the Relative Importance of Quasi-Biennial Oscillation and El Nino/Southern Oscillation in the Revised Dobson Total Ozone Records, J. Geophys. Res., 97 (D9), 10135–10144, 1992.

Zerefos, C., Contopoulos, G., and G. Skalkeas G. (Eds.): Twenty Years of Ozone Decline, Proceedings of the Symposium for the 20th Anniversary of the Montreal Protocol, Springer, Netherlands, Part of Springer Science + Business Media B. V, 470 pp., ISBN: 978-90-481-2468-8, 2009.

Zerefos, C. S., Kapsomenakis, J., Eleftheratos, K., Tourpali, K., Petropavlovskikh, I., Hubert, D., Godin-Beekmann, S., Steinbrecht, W., Frith, S., Sofieva, V., and Hassler, B.: Representativeness of single lidar stations for zonally averaged ozone profiles, their trends and attribution to proxies, Atmos. Chem. Phys., 18, 6427-6440, https://doi.org/10.5194/acp-18-6427-2018, 2018.

Zerefos, C. S., Tourpali, K, and Bais, A. F.: Further studies on possible volcanic signal to the ozone layer, J. Geophys. Res., 99 (D12), 25741–25746, 1994.

Zerefos, C. S., Tourpali, K, Isaksen, I. S. A., and Schuurmans, C. J. E.: Long term solar induced variation in total ozone, stratospheric temperatures and the tropopause, Adv. Space Res., 27 (12), 1943–1948, 2001.

Appendix A

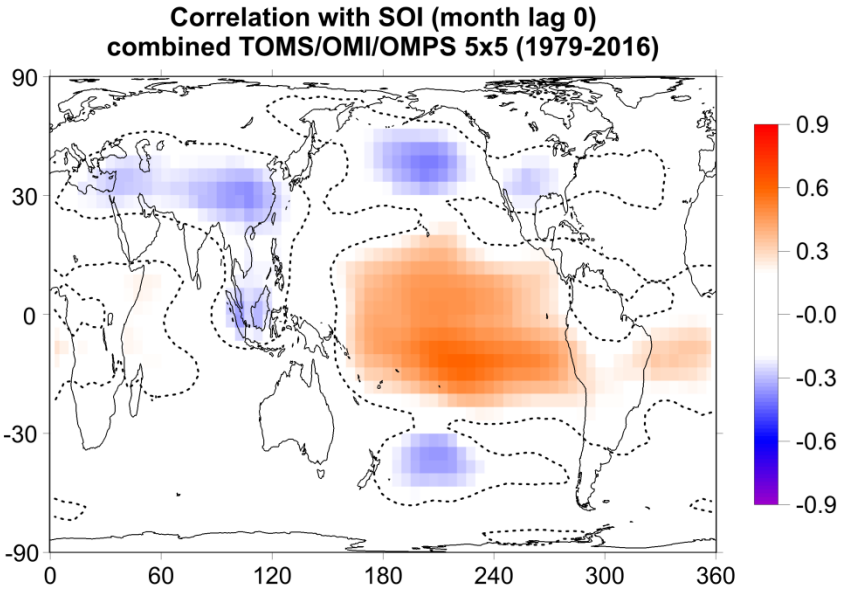

Figure A1. Map of correlation coefficients between total ozone from TOMS/OMI/OMPS satellite data and SOI for the whole period 1979-2016, after removing variability related to the seasonal cycle, QBO and solar cycle. The dotted line bounds the regions where the correlation coefficients are statistically significant at the 99% confidence level (t-test). Only correlation coefficients above/below ±0.2 are shown. Ozone data for the period 1991-1993 after the Mt Pinatubo eruption were not used in the correlation analysis to avoid any data contamination by the volcanic aerosols.

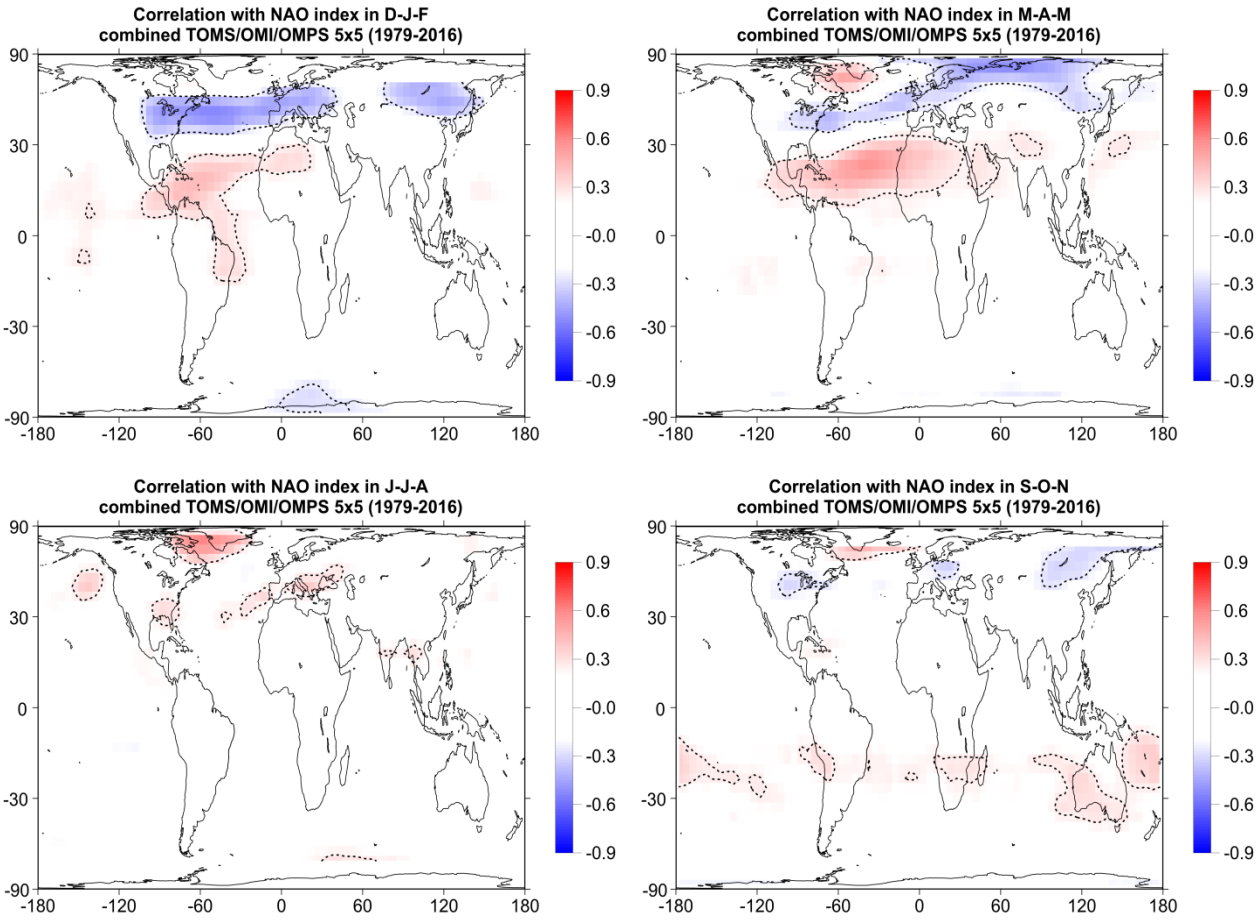

Figure A2. Map of correlation coefficients between total ozone from TOMS/OMI/OMPS satellite data and the NAO index during winter (December, January, February (D-J-F); upper left), spring (March, April, May (M-A-M); upper right), summer (June, July, August (J-J-A); lower left) and autumn (September, October, November (S-O-N); lower right) for the whole period 1979-2016, after removing variability related to the seasonal cycle, QBO, solar cycle and ENSO. The dotted line bounds the regions where the correlation coefficients are statistically significant at the 99% confidence level (t-test). Only correlation coefficients above/below ±0.2 are shown. Ozone data for the period 1991-1993 after the Mt Pinatubo eruption were not used in the correlation analysis to avoid any data contamination by the volcanic aerosols.

Table 1. Mean differences and their standard deviations in percent between total ozone from GOME-2A, SBUV (v8.6) satellite overpass data and ground-based observations over different latitude zones, as shown in Figures 1 and 2.

	[GOME-2A – SBUV] / SBUV (%) Stations mean data	[GOME-2A – GROUND] / GROUND (%) Stations mean data
60°-80° N	+1.3 ± 2.2	+2.5 ± 3.2
30°-60° N	+0.8 ± 1.6	+0.1 ± 1.9
0°-30° N	0.0 ± 0.7	–0.5 ± 1.2
0°-30° S	+0.1 ± 0.7	–0.9 ± 1.6
30°-60° S	+0.9 ± 1.6	0.0 ± 2.4
60°-80° S	–0.5 ± 2.9	0.0 ± 4.3

Table 2. Statistics of the correlations shown in Figures 1 and 2 between total ozone from a) GOME-2A data and SBUV (v8.6) overpass data, and b) GOME-2A data and ground-based measurements.

(a) GOME-2A and SBUV (v8.6)	Correlation	Intercept (DU)	Slope*	Error	t-value	p-value	N
60°-80° N	+0.987	4.925	0.999	0.015	65.224	<0.0001	117
30°-60° N	+0.984	5.002	0.993	0.017	59.784	<0.0001	118
0°-30° N	+0.989	28.304	0.894	0.012	72.404	<0.0001	118
0°-30° S	+0.981	21.575	0.919	0.017	53.874	<0.0001	118
30°-60° S	+0.977	–4.198	1.023	0.021	49.123	<0.0001	118
60°-80° S	+0.974	2.944	0.984	0.025	39.985	<0.0001	88

(b) GOME-2A and Ground-based	Correlation	Intercept (DU)	Slope*	Error	t-value	p-value	N
60°-80° N	+0.973	7.651	1.002	0.022	45.155	<0.0001	118
30°-60° N	+0.977	15.772	0.952	0.019	49.671	<0.0001	119
0°-30° N	+0.982	49.534	0.810	0.014	56.951	<0.0001	119
0°-30° S	+0.916	56.520	0.778	0.032	24.655	<0.0001	119
30°-60° S	+0.946	12.423	0.958	0.030	31.612	<0.0001	119
60°-80° S	+0.939	0.405	0.999	0.039	25.439	<0.0001	89

* Error, t-value and p-value refer to slope.

Table 3. Statistics of correlations between deseasonalized total ozone and the QBO at 30 hPa for a) GOME-2A data, b) GTO-ECV data, c) SBUV (v8.6) overpass data, and d) ground-based measurements.

(a) GOME-2A and QBO	Correlation	Intercept (%)	Slope*	Error	t-value	p-value	N
30°-60° N	–0.073	–0.045	–0.008	0.010	–0.791	0.4307	119
10°-30° N	–0.099	–0.048	–0.008	0.008	–1.077	0.2835	119
10° N-10° S	+0.767	0.654	0.114	0.009	12.910	<0.0001	119
10°-30° S	–0.472	–0.273	–0.048	0.008	–5.799	<0.0001	119
30°-60° S	–0.424	–0.262	–0.046	0.009	–5.063	<0.0001	119

(b) GTO-ECV and QBO	Correlation	Intercept (%)	Slope*	Error	t-value	p-value	N
30°-60° N	–0.116	–0.090	–0.012	0.007	–1.869	0.0628	259
10°-30° N	–0.142	–0.100	–0.014	0.006	–2.293	0.0226	259
10° N-10° S	+0.779	0.705	0.109	0.005	19.949	<0.0001	259
10°-30° S	–0.484	–0.306	–0.046	0.005	–8.873	<0.0001	259
30°-60° S	–0.417	–0.312	–0.048	0.007	–7.345	<0.0001	259

(b) SBUV v(8.6) and QBO	Correlation	Intercept (%)	Slope*	Error	t-value	p-value	N
30°-60° N	–0.165	–0.112	–0.018	0.007	–2.694	0.0075	262
10°-30° N	–0.177	–0.114	–0.018	0.006	–2.901	0.0040	263
10° N-10° S	+0.748	0.648	0.104	0.006	18.223	<0.0001	263
10°-30° S	–0.488	–0.287	–0.046	0.005	–9.037	<0.0001	263
30°-60° S	–0.458	–0.328	–0.051	0.006	–8.333	<0.0001	263

(b) Ground-based and QBO	Correlation	Intercept (%)	Slope*	Error	t-value	p-value	N
30°-60° N	–0.158	–0.123	–0.017	0.007	–2.594	0.0100	264
10°-30° N	–0.142	–0.083	–0.016	0.007	–2.317	0.0213	264
10° N-10° S	+0.695	0.553	0.095	0.006	15.327	<0.0001	253
10°-30° S	–0.490	–0.268	–0.046	0.005	–9.091	<0.0001	264
30°-60° S	–0.431	–0.322	–0.048	0.006	–7.734	<0.0001	264

* The slope is in % per unit change of the explanatory variable. Error, t-value and p-value refer to slope.

Table 4. Annual mean total ozone, amplitude of annual cycle, amplitude of QBO, amplitude of solar cycle and amplitude of ENSO in the period 1995-2016 from GOME-2A, GTO-ECV, the combined TOMS/OMI/OMPS satellite data and Oslo CTM3 model calculations over the South Pacific region (10^o-20^o S, 180^o-220^o E) and at station Samoa (14.25^o S, 189.4^o E) located within this region.

	South Pacific Ocean				station Samoa			
	GOME-2A*	GTO-ECV	TOMS/OMI/OMPS	Oslo CTM3	GOME-2A*	GTO-ECV	GROUND	SBUV (v8.6)
Annual mean	255.3 DU	254.7 DU	253.0 DU	259.5 DU	252.7 DU	252.2 DU	249.2 DU	251.9 DU
Amplitude of annual cycle	7.4 DU (2.9%)	7.7 DU (3.0%)	7.3 DU (2.9%)	5.2 DU (2.0%)	7.1 DU (2.8%)	6.7 DU (2.7%)	6.7 DU (2.7%)	7.3 DU (2.9%)
Amplitude of QBO	2.7 DU (1.0%)	2.2 DU (0.9%)	2.4 DU (0.9%)	2.3 DU (0.9%)	3.0 DU (1.2%)	2.2 DU (0.9%)	2.7 DU (1.1%)	2.0 DU (0.8%)
Amplitude of solar cycle	2.1 DU (0.8%)	4.1 DU (1.6%)	4.6 DU (1.8%)	1.8 DU (0.7%)	2.0 DU (0.8%)	4.5 DU (1.8%)	1.6 DU (0.6%)	4.5 DU (1.8%)
Amplitude of ENSO	6.2 DU (2.4%)	8.8 DU (3.5%)	6.0 DU (2.4%)	8.8 DU (3.4%)	5.6 DU (2.2%)	7.7 DU (3.0%)	5.5 DU (2.2%)	7.5 DU (3.0%)

*period 2007-2016

Table 5. Statistics of the comparisons between total ozone, tropopause pressures and SOI for a) South Pacific (10°-20° S, 180°-220° E), b) station Samoa (14.25° S, 189.4° E), c) South Asia (35°-45° N, 45°-125° E) and d) 7 stations in South Asia.

(a) South Pacific	Correlation with SOI	Intercept (%)	Slope*	Error	t-value	p-value	N
GOME-2A	+0.56	–0.238	0.118	0.016	7.236	<0.0001	119
GTO-ECV	+0.66	–0.069	0.145	0.010	14.014	<0.0001	252
TOMS/OMI/OMPS	+0.62	–0.139	0.134	0.011	12.285	<0.0001	241
Oslo CTM3	+0.55	–0.064	0.144	0.014	10.501	<0.0001	252
Tropopause	+0.66	–0.761	0.241	0.017	13.825	<0.0001	252

(b) Samoa	Correlation with SOI	Intercept (%)	Slope*	Error	t-value	p-value	N
GOME-2A	+0.47	–0.217	0.108	0.018	5.823	<0.0001	119
GTO-ECV	+0.55	–0.100	0.127	0.012	10.366	<0.0001	252
SBUV overpass	+0.59	–0.114	0.127	0.011	11.398	<0.0001	251
GB (WOUDC)	+0.42	–0.058	0.106	0.017	6.194	<0.0001	178
Tropopause	+0.65	–0.799	0.223	0.017	13.405	<0.0001	252

(c) South Asia	Correlation with SOI	Intercept (%)	Slope*	Error	t-value	p-value	N
GOME-2A	–0.23	0.090	–0.044	0.018	–2.525	0.0129	119
GTO-ECV	–0.30	0.073	–0.074	0.015	–5.047	<0.0001	252
TOMS/OMI/OMPS	–0.28	–0.212	–0.073	0.016	–4.553	<0.0001	241
Oslo CTM3	–0.18	0.140	–0.040	0.014	–2.877	0.0044	252
Tropopause	–0.27	–0.188	–0.129	0.029	–4.476	<0.0001	252

(d) South Asia (7 stations mean)	Correlation with SOI	Intercept (%)	Slope*	Error	t-value	p-value	N
GOME-2A	–0.23	0.090	–0.043	0.017	–2.518	0.0132	119
GTO-ECV	–0.30	0.067	–0.072	0.014	–5.040	<0.0001	252
SBUV overpass	–0.27	0.086	–0.066	0.015	–4.464	<0.0001	251
GB (WOUDC)	–0.36	0.427	–0.103	0.017	–5.912	<0.0001	240
Tropopause	–0.28	–0.122	–0.160	0.035	–4.597	<0.0001	252

* The slope is in % per unit change of the explanatory variable. Error, t-value and p-value refer to slope.

Table 6. Annual mean total ozone, amplitude of annual cycle, amplitude of QBO, amplitude of solar cycle and amplitude of NAO in the period 1995-2016 from GOME-2A, GTO-ECV, the combined TOMS/OMI/OMPS satellite data and Oslo CTM3 model calculations over the North Atlantic Ocean: (a) region 35°-50° N, 20°-50° W, and (b) region 15°-27° N, 30°-60° W.

	North Atlantic Ocean							
	(a) 35°-50° N, 20°-50° W				(b) 15°-27° N, 30°-60° W			
	GOME-2A*	GTO-ECV	TOMS/OMI/OMPS	Oslo CTM3	GOME-2A*	GTO-ECV	TOMS/OMI/OMPS	Oslo CTM3
Annual mean	319.7 DU	315.9 DU	317.3 DU	311.2 DU	276.6 DU	276.4 DU	274.4 DU	282.6 DU
Amplitude of annual cycle	37.4 DU (11.7%)	37.0 DU (11.7%)	36.9 DU (11.6%)	32.0 DU (10.3%)	12.7 DU (4.6%)	15.8 DU (5.7%)	15.1 DU (5.5%)	15.5 DU (5.5%)
Amplitude of QBO	2.5 DU (0.8%)	2.3 DU (0.7%)	2.6 DU (0.8%)	3.2 DU (1.0%)	3.0 DU (1.1%)	2.8 DU (1.0%)	3.9 DU (1.4%)	4.3 DU (1.5%)
Amplitude of solar cycle	0.4 DU (0.1%)	0.3 DU (0.1%)	2.2 DU (0.7%)	2.3 DU (0.7%)	3.5 DU (1.3%)	2.7 DU (1.0%)	3.3 DU (1.2%)	1.0 DU (0.3%)
Amplitude of NAO (winter)	18.3 DU (5.7%)	16.5 DU (5.2%)	18.4 DU (5.8%)	18.3 DU (5.9%)	4.2 DU (1.5%)	7.2 DU (2.6%)	5.0 DU (1.8%)	8.0 DU (2.8%)

*period 2007-2016

Table 7. Annual mean total ozone, amplitude of annual cycle, amplitude of QBO, amplitude of solar cycle and amplitude of NAO in the period 1995-2016 from GOME-2A, GTO-ECV satellite data, ground-based observations and SBUV (v8.6) satellite overpass data over: (a) Canada and USA (11 stations mean), and (b) Europe (41 stations mean).

	(a) Canada and USA				(b) Europe			
	30^o-50^o N, 60^o-110^o W (11 stations mean)				35^o-55^o N, 10^o W-40^o E (41 stations mean)			
	GOME-2A*	GTO-ECV	GROUND	SBUV (v8.6)	GOME-2A*	GTO-ECV	GROUND	SBUV (v8.6)
Annual mean	324.2 DU	320.6 DU	322.5 DU	320.9 DU	329.9 DU	325.7 DU	326.9 DU	326.8 DU
Amplitude of annual cycle	38.1 DU (11.7%)	34.1 DU (10.6%)	33.2 DU (10.3%)	34.0 DU (10.6%)	39.3 (11.9%)	40.5 DU (12.4%)	39.2 DU (12.0%)	40.7 DU (12.4%)
Amplitude of QBO	2.1 DU (0.6%)	2.5 DU (0.8%)	3.5 DU (1.1%)	2.6 DU (0.8%)	2.7 DU (0.8%)	1.9 DU (0.6%)	2.8 DU (0.8%)	2.2 DU (0.7%)
Amplitude of solar cycle	0.3 DU (0.1%)	0.5 DU (0.2%)	1.4 DU (0.4%)	0.5 DU (0.2%)	2.1 DU (0.6%)	0.8 DU (0.2%)	1.0 DU (0.3%)	0.3 DU (0.1%)
Amplitude of NAO (winter)	9.8 DU (3.0%)	6.9 DU (2.2%)	8.7 DU (2.7%)	9.3 DU (2.9%)	9.8 DU (3.0%)	8.9 DU (2.7%)	11.8 DU (3.6%)	9.9 DU (3.0%)

*period 2007-2016

844

845 **Table 8. Statistics of the comparisons between total ozone, tropopause pressures and NAO index in winter**
846 **(DJF mean) for a) the northern part of North Atlantic (35°-50° N, 20°-50° W), b) its southern part (15°-27° N,**
847 **30°-60° W), c) 11 stations in Canada and USA, and d) 41 stations in Europe.**

848

(a) Northern part of North Atlantic	Correlation with NAO in winter	Intercept (%)	Slope*	Error	t-value	p-value	N
GOME-2A	–0.85	0.035	–2.474	0.568	–4.355	0.0033	9
GTO-ECV	–0.74	0.412	–2.188	0.453	–4.827	0.0001	21
TOMS/OMI/OMPS	–0.74	0.734	–2.386	0.538	–4.436	0.0004	18
Oslo CTM3	–0.75	0.639	–2.457	0.498	–4.937	<0.0001	21
Tropopause	–0.83	0.665	–3.112	0.480	–6.478	<0.0001	21

849

(b) Southern part of North Atlantic	Correlation with NAO in winter	Intercept (%)	Slope*	Error	t-value	p-value	N
GOME-2A	+0.54	–0.132	0.661	0.386	1.712	0.1306	9
GTO-ECV	+0.60	–0.202	1.097	0.333	3.291	0.0038	21
TOMS/OMI/OMPS	+0.58	–0.334	1.138	0.402	2.832	0.0120	18
Oslo CTM3	+0.65	–0.077	1.188	0.316	3.761	0.0013	21
Tropopause	+0.59	–0.702	1.547	0.482	3.207	0.0046	21

850

(a) CA/USA (11 stations mean)	Correlation with NAO in winter	Intercept (%)	Slope*	Error	t-value	p-value	N
GOME-2A	–0.71	–0.042	–1.305	0.493	–2.647	0.0331	9
GTO-ECV	–0.40	0.308	–0.904	0.479	–1.886	0.0746	21
SBUV overpass	–0.50	0.318	–1.209	0.476	–2.541	0.0199	21
GB (WOUDC)	–0.46	0.268	–1.046	0.477	–2.190	0.0419	20
Tropopause	–0.41	0.268	–0.739	0.377	–1.959	0.0650	21

851

(b) Europe (41 stations mean)	Correlation with NAO in winter	Intercept (%)	Slope*	Error	t-value	p-value	N
GOME-2A	–0.46	0.089	–1.282	0.897	–1.428	0.1963	9
GTO-ECV	–0.42	0.315	–1.141	0.573	–1.992	0.0609	21
SBUV overpass	–0.47	0.389	–1.264	0.543	–2.329	0.0311	21
GB (WOUDC)	–0.48	0.625	–1.327	0.560	–2.368	0.0287	21
Tropopause	–0.40	0.048	–0.989	0.523	–1.891	0.0739	21

852 * The slope is in % per unit change of the explanatory variable. Error, t-value and p-value refer to slope,

853

854
855

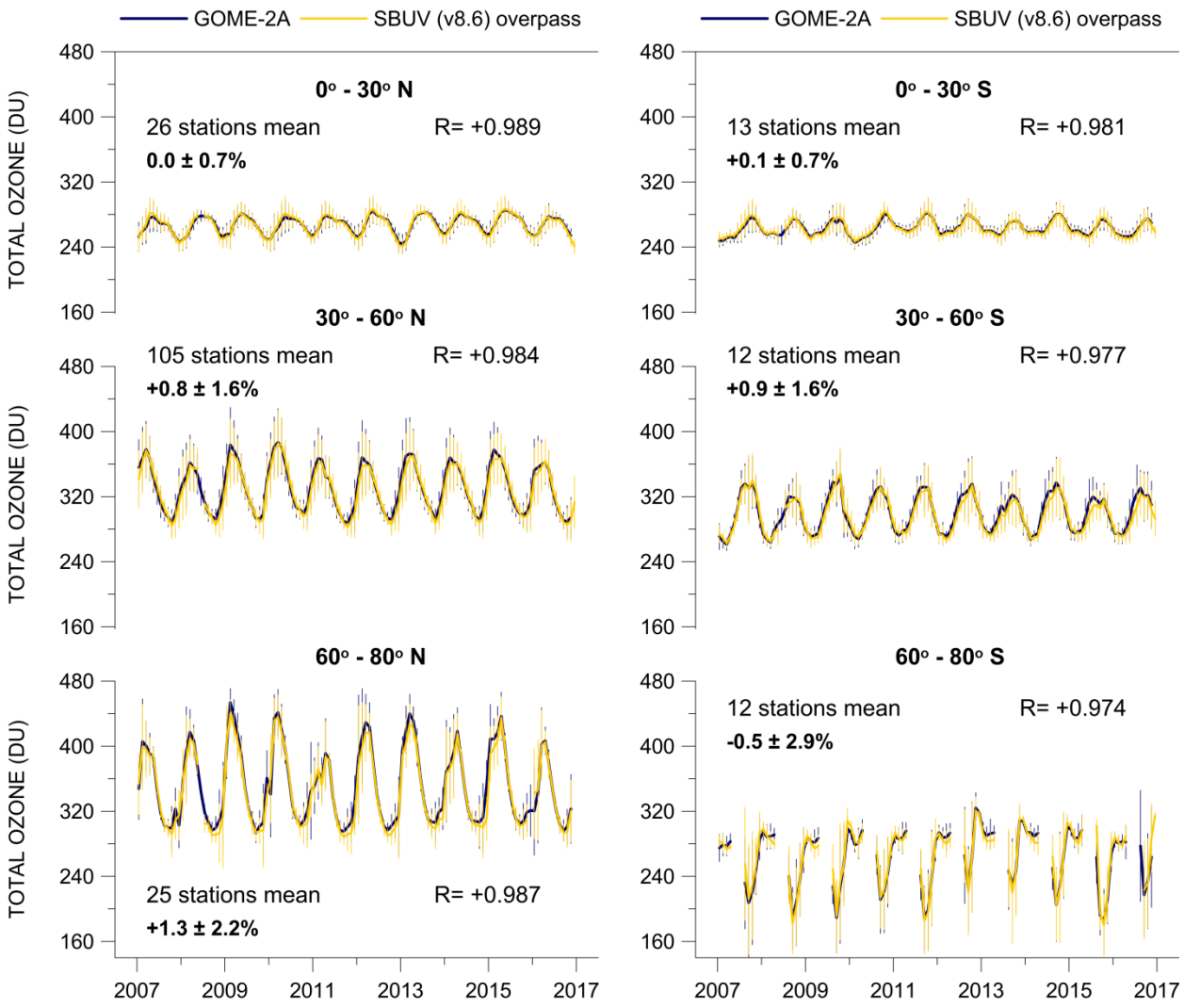

Figure 1. Monthly mean total ozone from GOME-2A as compared with monthly mean total ozone from SBUV (v8.6) satellite overpass data for the period 2007-2016 over the Northern and the Southern Hemisphere based on stations mean data. *R* is the correlation coefficient between the two lines. Error bars show the standard deviation of each monthly mean. Mean differences ± σ are given as [GOME-2A – SBUV] / SBUV (%).

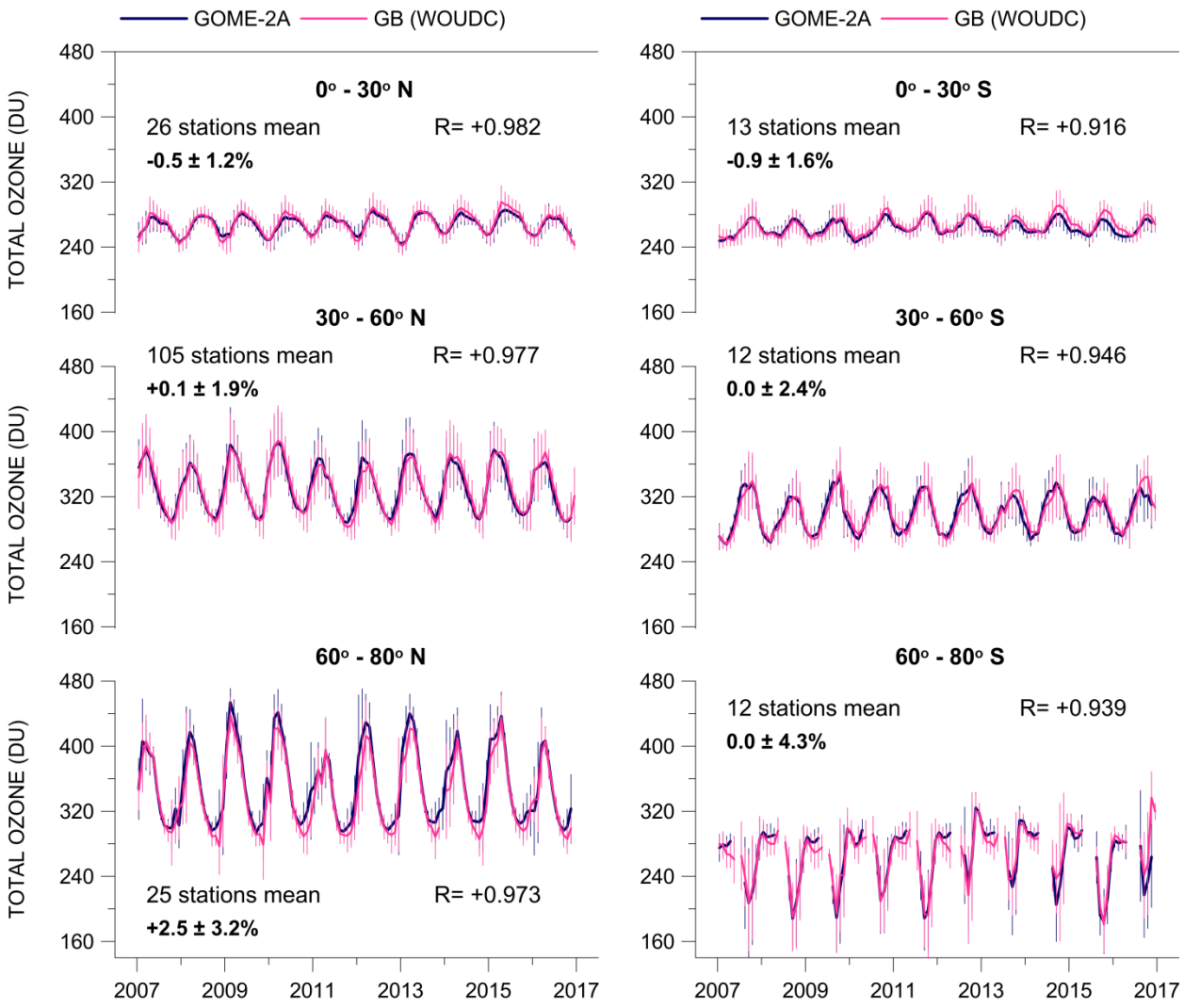

Figure 2. Same as in Figure 1 but for GOME-2A and GB observations. *R* is the correlation coefficient between the two lines. Error bars show the standard deviation of each monthly mean. Mean differences ± σ are given as [GOME-2A – GROUND] / GROUND (%).

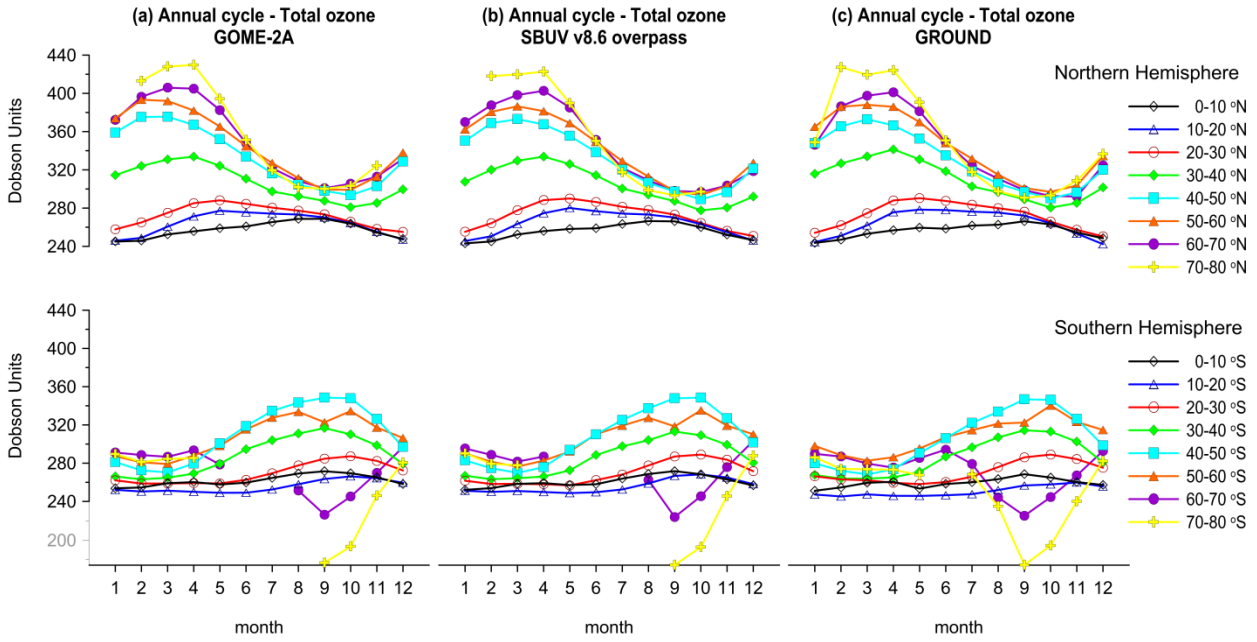

Figure 3. Comparison of the annual cycle of total ozone from GOME-2A with that from SBUV (v8.6) satellite overpass data and GB observations in the period 2007-2016 based on stations data averaged per 10 degree latitude zones. The annual cycle is distorted above 60 deg. S due to the Antarctic ozone hole.

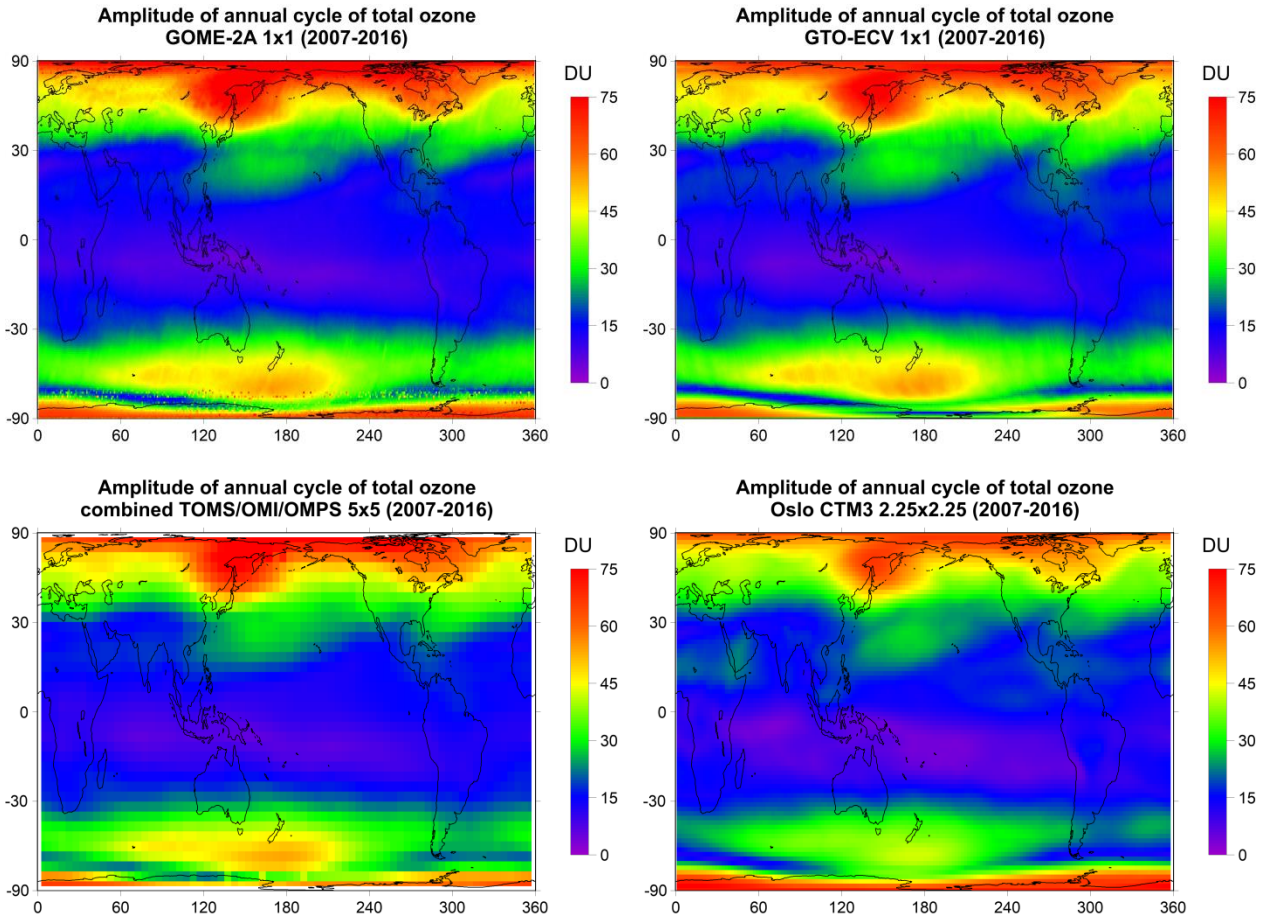

Figure 4. Comparison of the amplitude [i.e., (max-min)/2] of the annual cycle of total ozone from GOME-2A (upper left) with the amplitude of the annual cycle of total ozone from GTO-ECV (upper right), the combined TOMS/OMI/OMPS satellite data (lower left) and Oslo CTM3 model simulations (lower right).

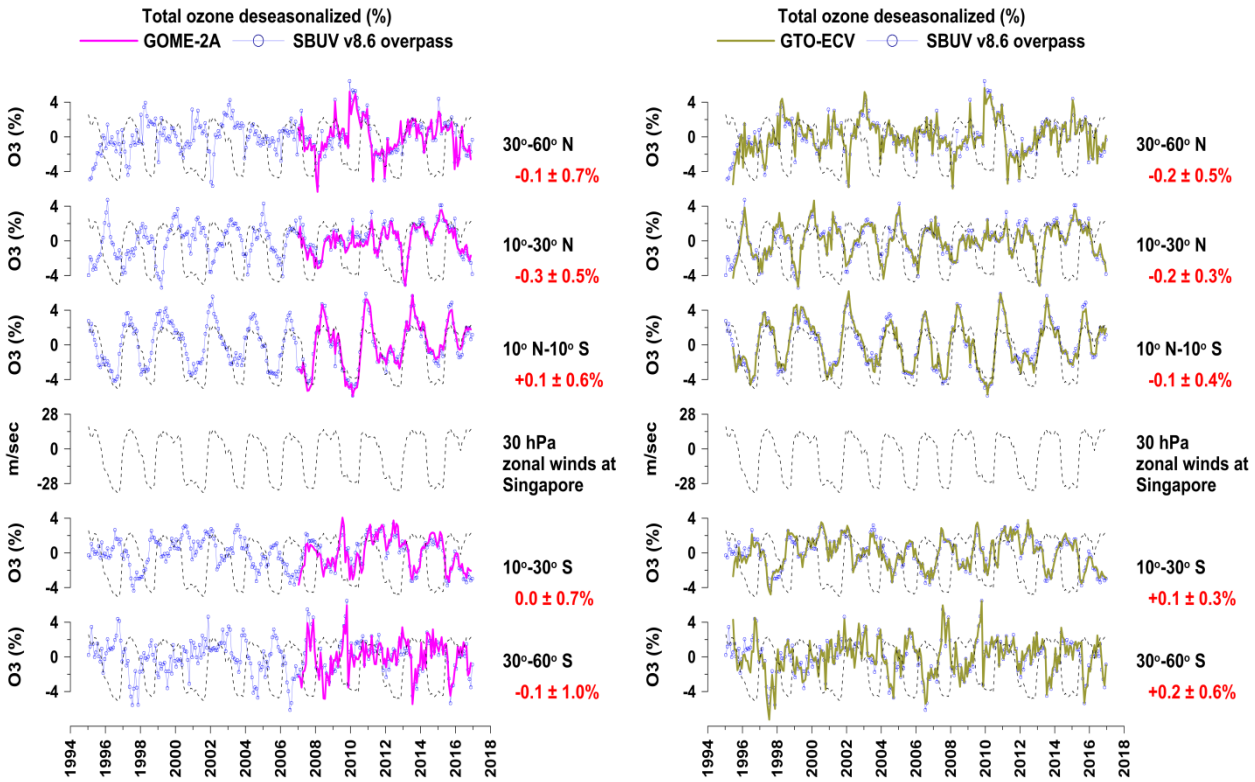

Figure 5. (Left panel) Time series of deseasonalised total ozone from GOME-2A and SBUV (v8.6) satellite overpasses over different latitude zones along with the equatorial zonal winds at 30 hPa as an index of the QBO; (Right panel) same as in left panel but for GTO-ECV and SBUV. Values with red colour refer to the mean differences ± σ (in %) between GOME-2A and SBUV deseasonalised data averaged over various WOUDC stations (150 stations in the northern mid-latitudes (30°-60° N), 21 stations in the northern subtropics (10°-30° N), 8 stations in the tropics (10° S-10° N), 10 stations in southern subtropics (10°-30° S) and 12 stations in the southern mid-latitudes (30°-60° S)). The QBO proxy is superimposed on the ozone anomalies.

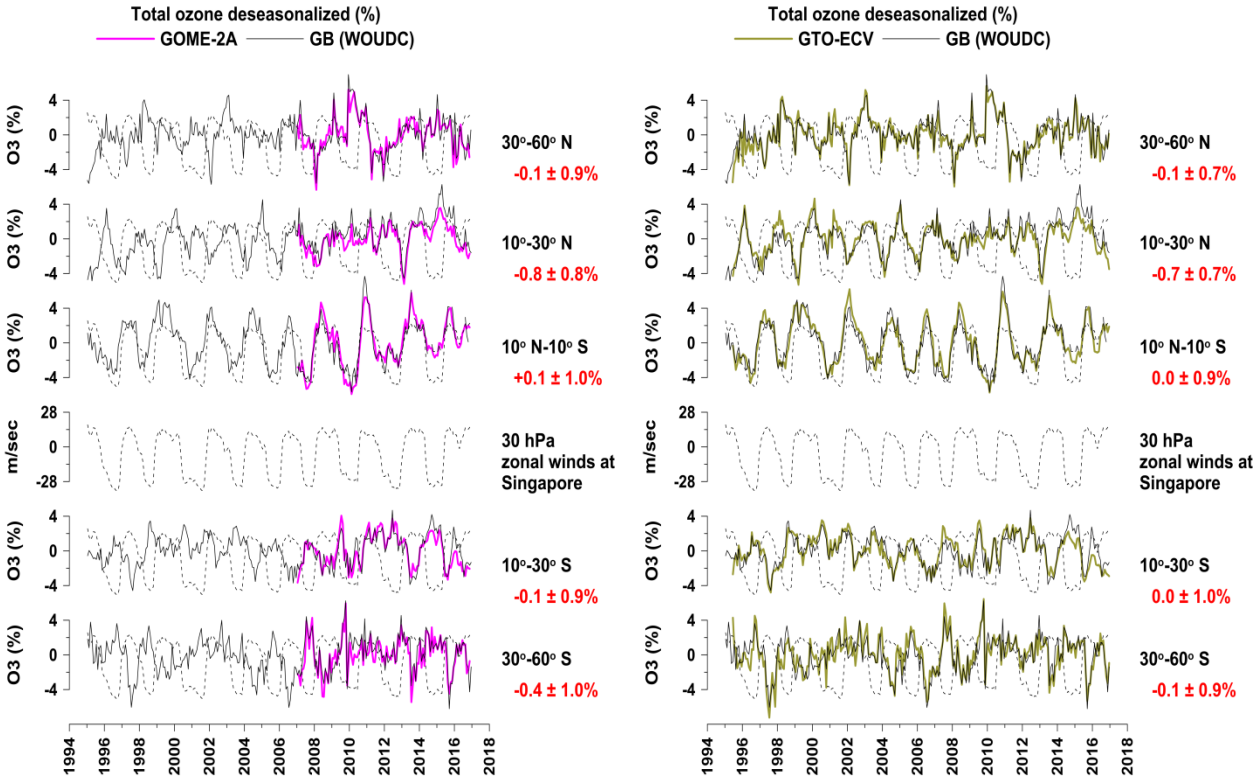

Figure 6. Same as in Figure 5 but for GOME-2A and GB observations (left panel), and for GTO-ECV and GB observations (right panel). The QBO proxy is superimposed on the ozone anomalies.

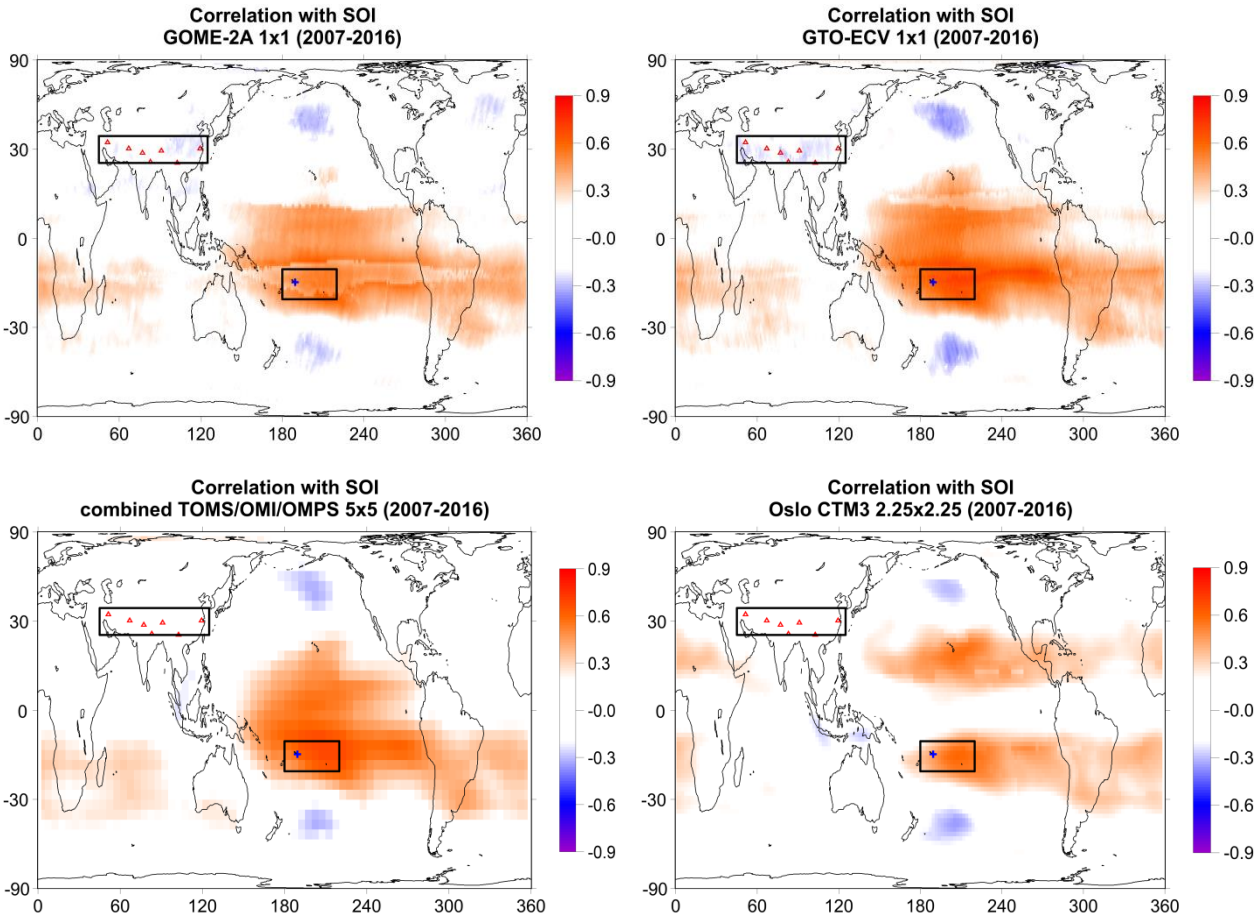

Figure 7. Map of correlation coefficients between total ozone and SOI for GOME-2A (upper left), GTO-ECV (upper right), TOMS/OMI/OMPS satellite data (lower left) and Oslo CTM3 model simulations (lower right). Rectangles correspond to the South Pacific region (10-20 ^{o}S, 180-220 ^{o}E) and South Asia region (35-45 ^{o}N, 45-125 ^{o}E), blue cross to the station Samoa (14.25 ^{o}S, 189.4 ^{o}E) and red triangles to stations in South Asia, in which total ozone has been studied as for the impact of ENSO after removing variability related to the annual cycle, QBO and solar cycle. Positive correlations are shown by red colours while negative correlations by blue colours. Only correlation coefficients above/below ±0.2 are shown.

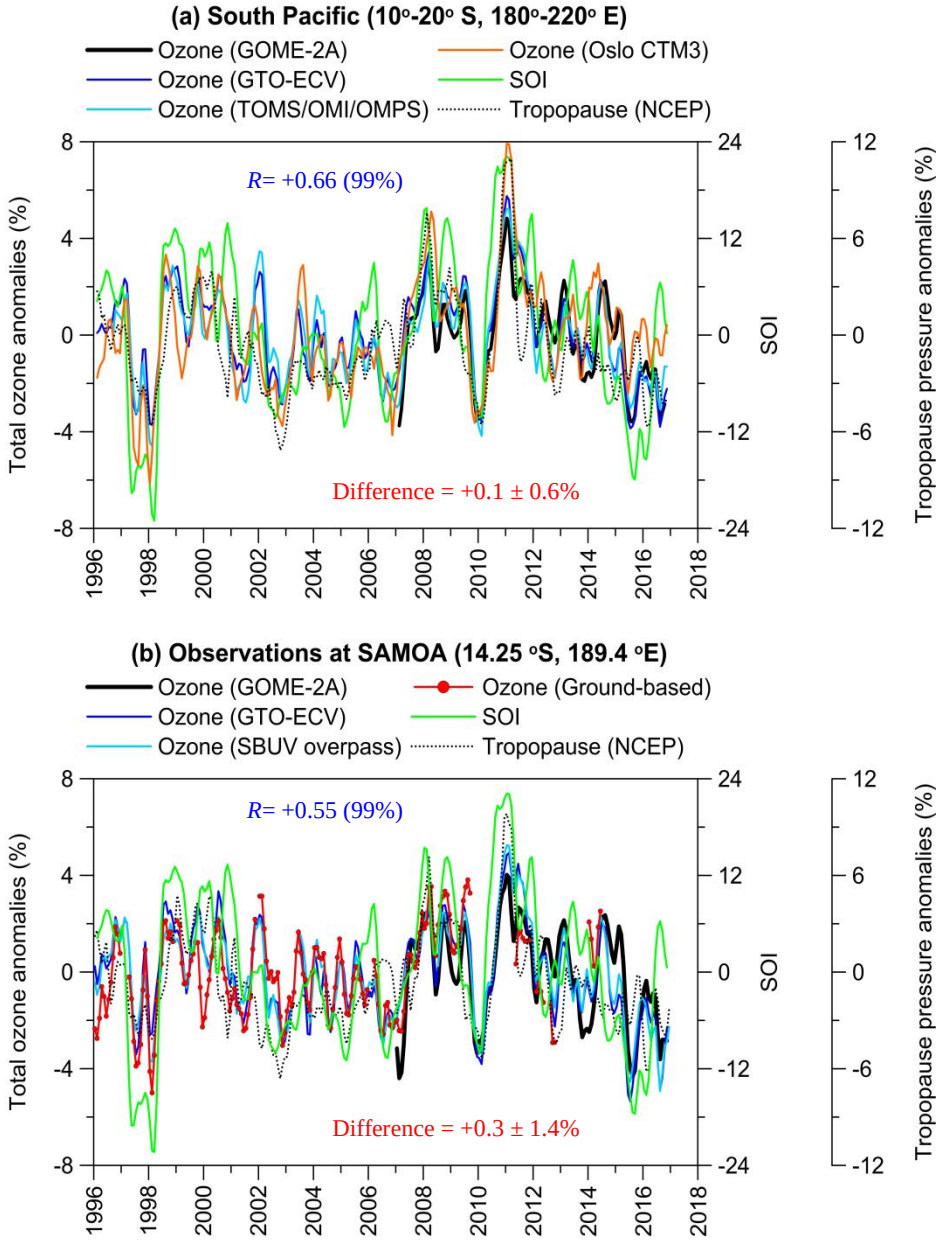

Figure 8. (a) Example of regional time series of total ozone (%) over the South Pacific region (10°-20° S, 180°-220° E) along with SOI. The dotted line shows the respective tropopause pressure variability from NCEP. *R* is the correlation coefficient between GTO-ECV total ozone and SOI (statistical significance of *R* is given in parentheses). The difference refers to the mean difference ± σ (in %) between GTO-ECV and the combined TOMS/OMI/OMPS satellite data. (b) Same as in (a) but for SBUV overpass and GB data at the station Samoa. The difference refers to the mean difference ± σ (in %) between GTO-ECV and GB data.

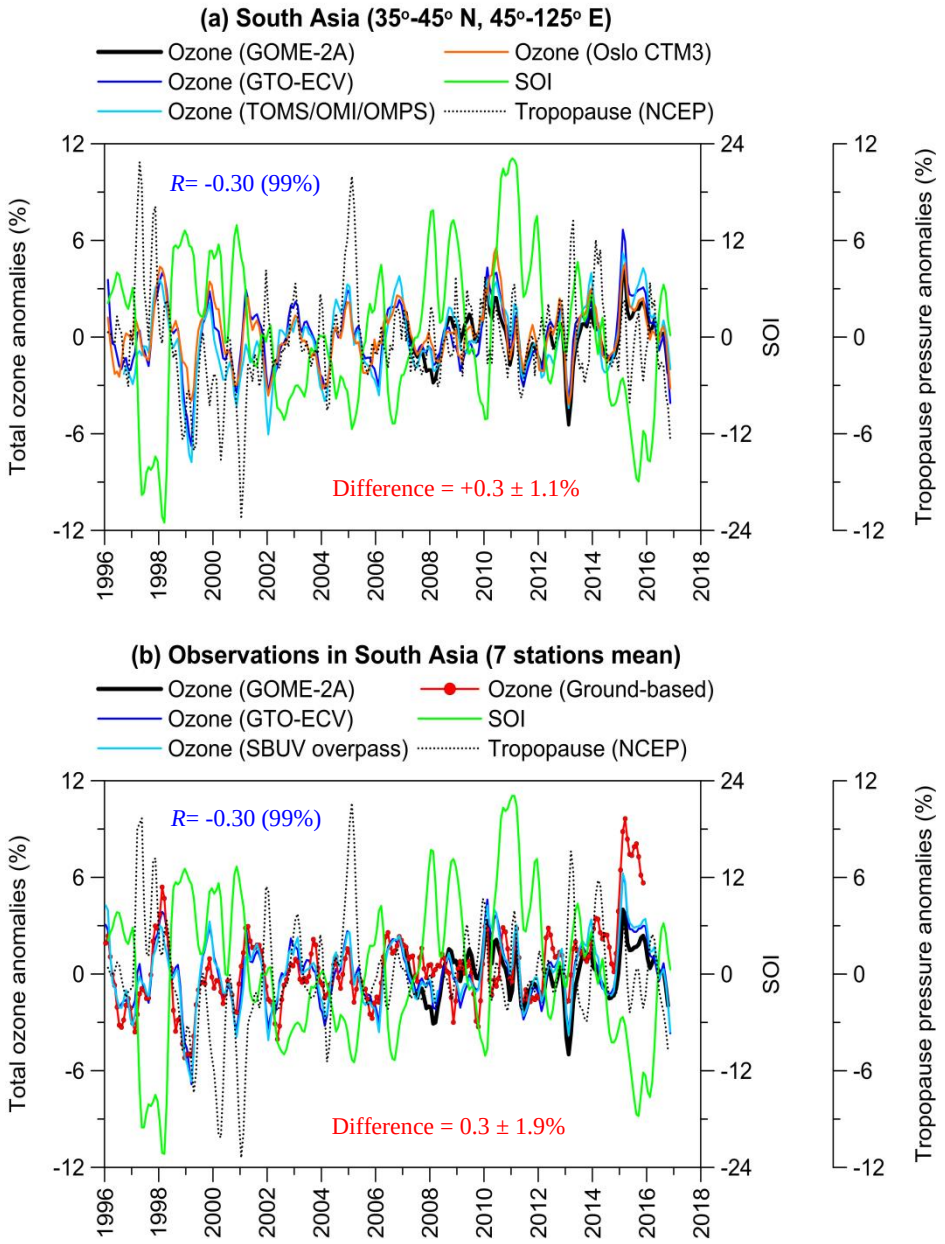

Figure 9. (a) Example of regional time series of total ozone (%) over South Asia (35°-45° N, 45°-125° E) along with SOI. The dotted line shows the respective tropopause pressure variability from NCEP. *R* is the correlation coefficient between GTO-ECV total ozone and SOI (statistical significance of *R* is given in parentheses). The difference refers to the mean difference ± σ (in %) between GTO-ECV and the combined TOMS/OMI/OMPS satellite data. (b) Same as in (a) but with SBUV overpass and GB data averaged at 7 stations in South Asia. The difference refers to the mean difference ± σ (in %) between GTO-ECV and GB data.

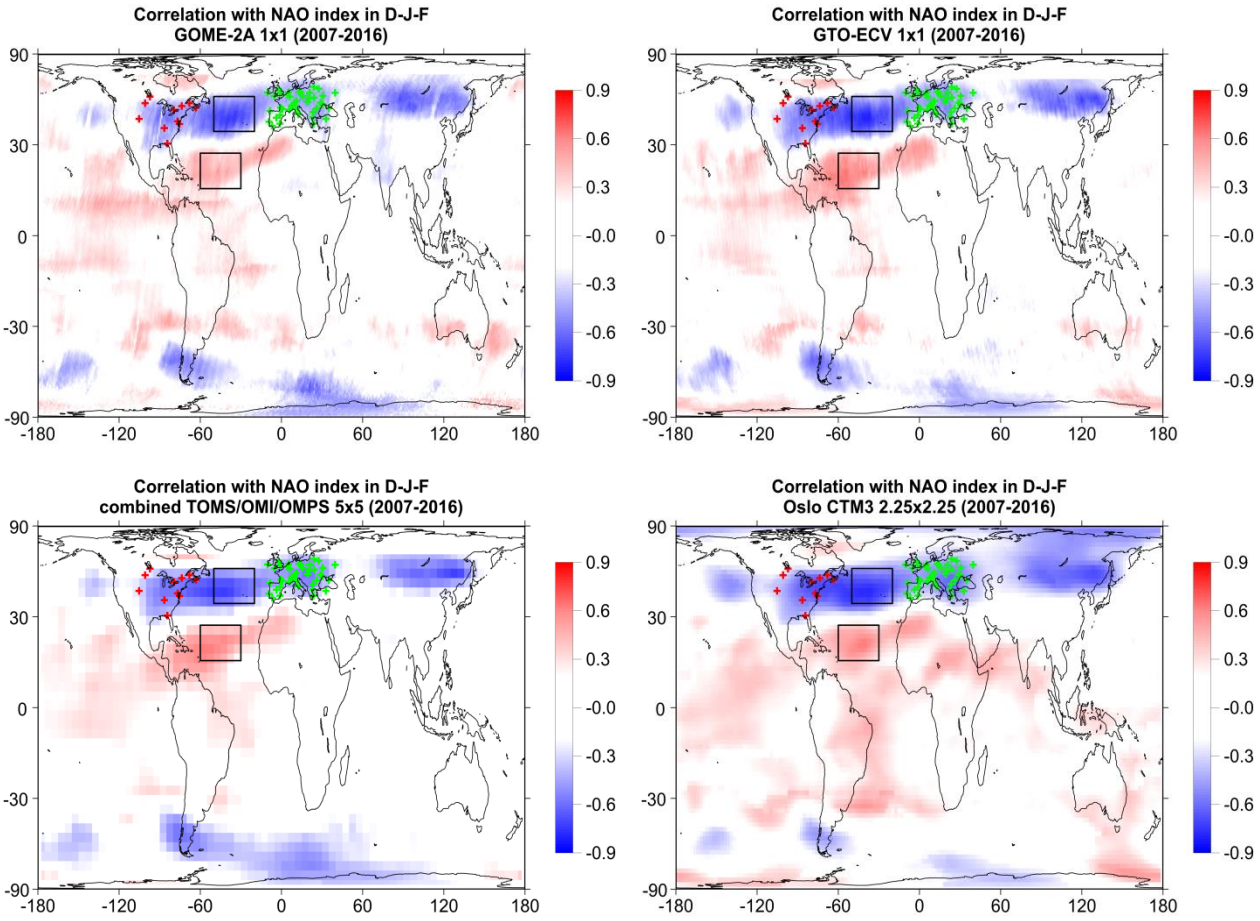

Figure 10. Map of correlation coefficients between total ozone and the NAO index during winter (December, January, February; D-J-F) for GOME-2A (upper left), GTO-ECV (upper right), TOMS/OMI/OMPS satellite data (lower left) and Oslo CTM3 model simulations (lower right). Rectangles correspond to regions in the North Atlantic (35°-50° N, 20°-50° W; 15°-27° N, 30°-60° W), and red and green crosses to stations in Canada/USA and Europe, in which total ozone has been studied as for the impact of NAO after removing variability related to the annual cycle , QBO, solar cycle and ENSO. Positive correlations are shown by red colours while negative correlations by blue colours. Only correlation coefficients above/below ±0.2 are shown.

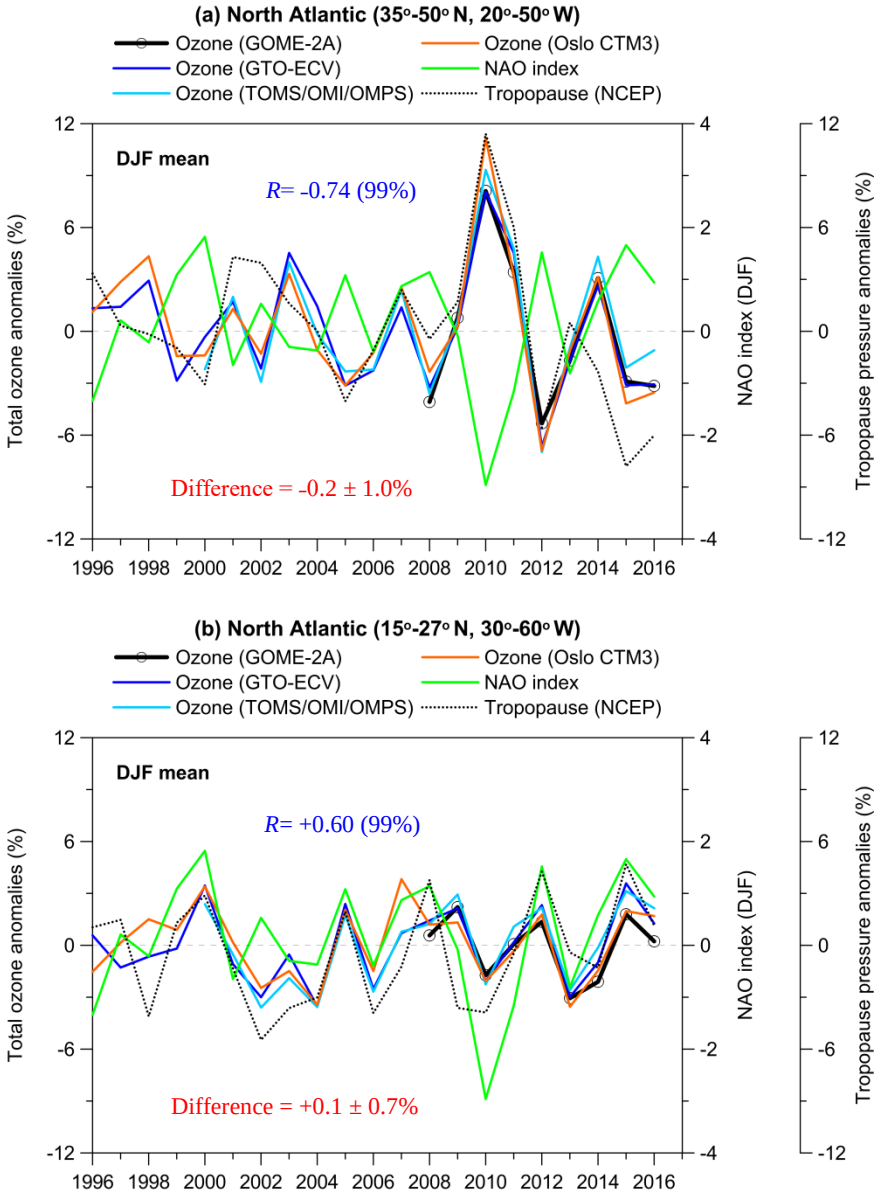

Figure 11. Example of regional time series of total ozone (%) over the North Atlantic regions (a) 35°-50° N, 20°-50° W and (b) 15°-27° N, 30°-60° W in winter (DJF mean) along with the NAO index. The dotted line shows the respective tropopause pressure variability from NCEP reanalysis. *R* is the correlation coefficient between GTO-ECV total ozone and the NAO index. The differences refer to the mean differences ± σ (in %) between GTO-ECV and the combined TOMS/OMI/OMPS satellite data.

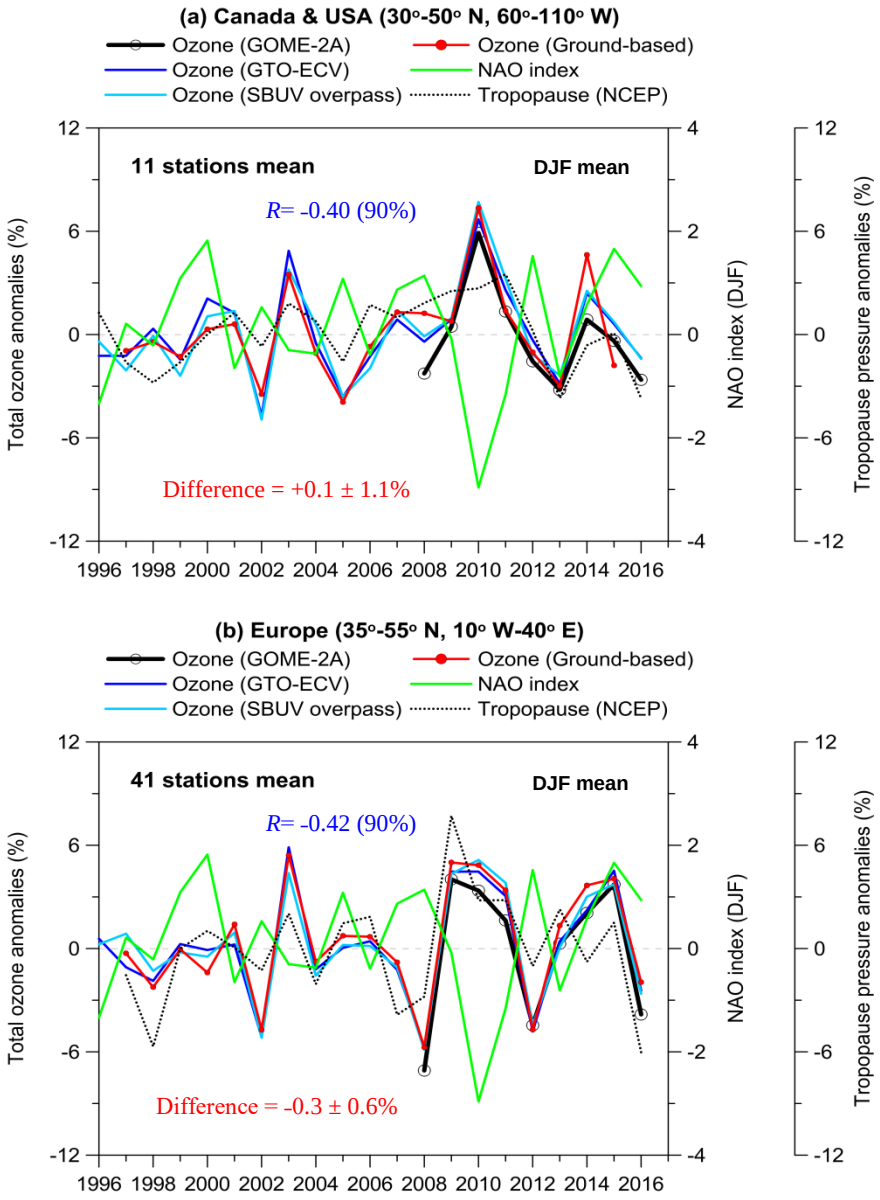

Figure 12. Comparison with GB observations over: (a) Canada and USA and (b) Europe in winter (DJF mean). *R* is the correlation coefficient between GTO-ECV total ozone and the NAO index. The differences refer to the mean differences ± σ (in %) between GTO-ECV and GB data.

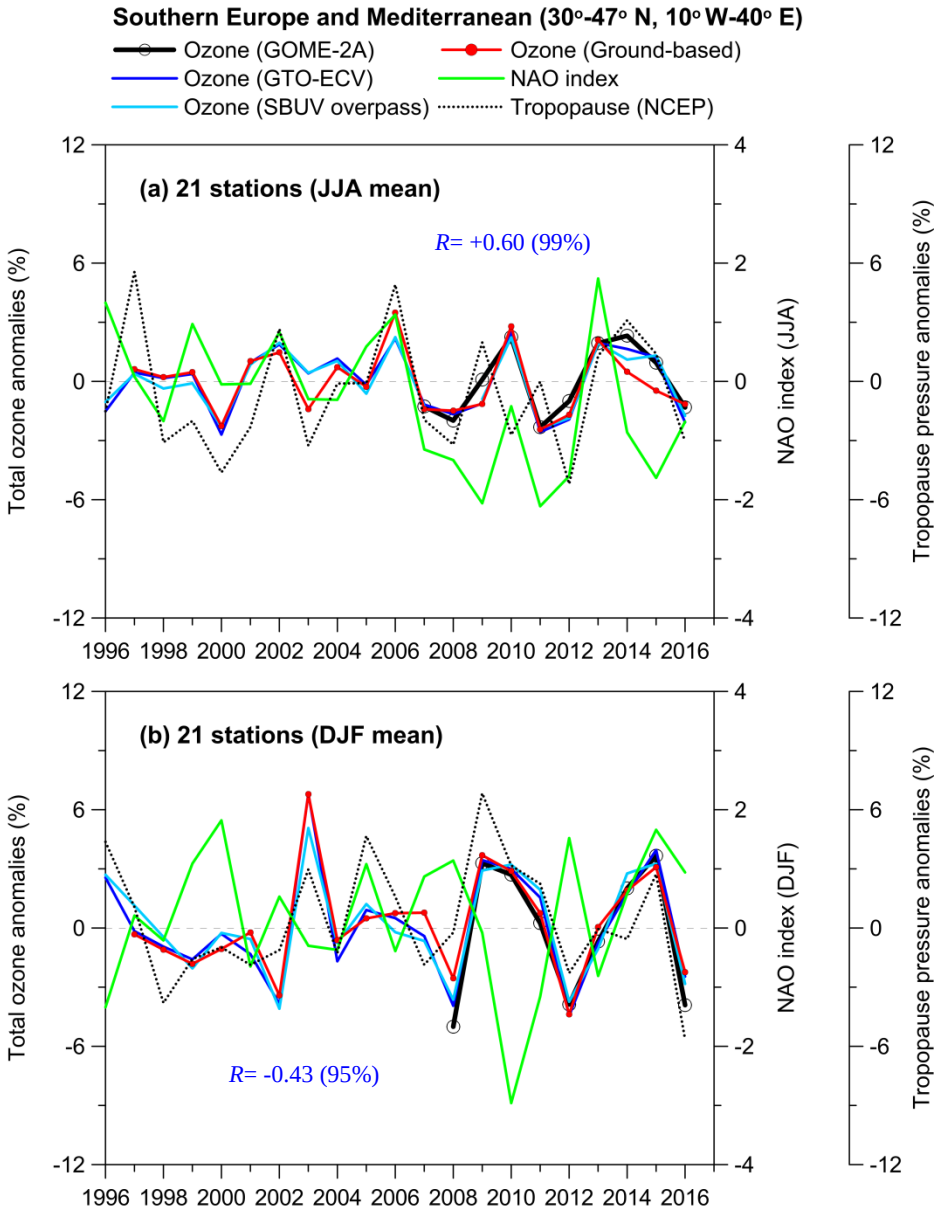

Figure 13. Relation between total ozone and the NAO index in summer (JJA mean) and winter (DJF mean) for 21 stations in southern Europe. The correlation coefficients refer to NAO index and GB total ozone after removing variability related to the seasonal cycle, QBO, solar cycle and ENSO.